

**CAN EFFECTIVE MANAGEMENT OF RIPARIAN ZONE  
VEGETATION SIGNIFICANTLY REDUCE THE COST OF  
CATCHMENT MANAGEMENT AND ENABLE GREATER  
PRODUCTIVITY OF LAND RESOURCES**

Research Organisation:

**DIVISION OF WATER ENVIRONMENT AND FORESTRY  
TECHNOLOGY (ENVIRONMENTEK) CSIR**

**Project Number : K5/1284  
Project leader : C. Everson  
Report : September 2005**

**Project Team: C. Everson, M. Moodley, M. Gush, C. Jarman, M.  
Govender and P. Dye**

# CONTENTS

<b>CHAPTER 1: INTRODUCTION</b> .....	4
<b>CHAPTER 2: THE STUDY AREA</b> .....	6
<b>2.1 Study site.</b> .....	7
<b>CHAPTER 3: METHODS AND MATERIALS</b>	
<b>3.1 Rainfall</b> .....	9
<b>3.2 General climatic conditions</b> .....	9
<b>3.3 Streamflow</b> .....	9
<b>3.4 Ground Water Monitoring</b> .....	9
<b>3.5 Soil Water dynamics</b> .....	9
<b>3.6 Evaporation monitoring</b> .....	11
3.6.1 Description of the Heat pulse velocity technique.....	11
3.6.1.1 Theory of the HPV technique.....	11
3.6.1.2 The HPV equipment .....	12
3.6.1.3 Patching of the HPV data .....	12
3.6.1.4 Application of the HPV technique to <i>A, mearsniii</i>	13
3.6.2 Bowen ratio energy balance technique	
3.6.2.1 Theory.....	14
3.6.2.2 Instrumentation .....	14
3.6.2.3 Installation of the BREB equipment.....	14
<b>3.7 Geophysical survey: Ground Penetrating Radar</b> .....	15
3.7.1 Mapping the bedrock profile .....	15
<b>3.8 Site management</b> .....	17
<b>CHAPTER 4: Results and Discussion</b>	
<b>4.1 Rainfall monitoring</b> .....	18
<b>4.2 Streamflow gauging</b> .....	29
<b>4.3 Soil Water Monitoring</b> .....	22
4.3.1 Soil properties.....	22
<b>4.4 Ground Water Monitoring</b> .....	29
<b>4.5 Surface runoff</b> .....	30
<b>4.6 Sap flow studies in the wattle trees</b> .....	30
<b>4.7 Grassland evaporation in the riparian zone</b> .....	32
<b>4.8 Geophysical survey using GPR</b> .....	33
<b>4.9 Catchment scale modelling</b> .....	34
4.9.1 Introduction.....	34
4.9.2 Background to the SWAT model .....	34
4.9.3 Data Sources .....	35
4.9.4 Model Configuration .....	35
4.9.5 Results .....	36
<b>4.10 Conclusions</b> .....	38
<b>5. Acknowledgments</b> .....	38

# Chapter 1

## Introduction

Wetlands are a common feature of all landscapes, manifesting themselves as ponds, springs, seeps, bogs and mires to mention just a few. Of interest in this report is the interconnection of wetlands through river channels (with riverbanks), which can be broadly defined as riparian habitats. The economic and ecological importance of wetlands is well recognised internationally. Despite this recognition, it is estimated that over 50% of South Africa's wetlands have already been destroyed. The main cause has been the drainage of wetlands for crops and pastures, overgrazing, planting of alien trees in riparian zones and urban development. Since wetlands play such a vital role in the hydrology of catchments (attenuation of floods, prevention of soil erosion, removal of pollutants, plus many more) their importance and function has been recognised in the National Water Act of 1998. In the Act riparian habitat is defined as the physical structure and associated vegetation for the areas associated with a water course which are commonly characterised by alluvial soils and which are inundated or flooded to an extent and with a frequency sufficient to support vegetation of species with a composition and physical structure distinct from those adjacent land areas.

Riparian habitats often represent the deepest, most fertile soils in a catchment, and the high soil water contents make it an ideal site for plant establishment and growth. For these reasons riparian zones normally produce the highest growth rates of commercially planted trees, making them vulnerable to exploitation by the forest industry. Since growing trees in the riparian zone results in a decrease in riparian functioning (through increased water use and loss of biodiversity), the forest industry has adopted a proactive approach to optimise water use, primarily by protecting the riparian zone (Woodborne, Robertson & February 2003). This was formalised in the 1969 Soil Conservation Act, and the Amendment of the Forestry Act (1968) further restricted afforestation in riparian habitats to no closer than 20 m from stream banks. Because of the loss of these highly productive riparian areas to the forest industry, riparian zone management has become an important issue in water conservation in South Africa and water resource managers are under increasing pressure to assess the impact of different land uses and management practices on catchment water yield. The need to exclude plantation trees from riparian zones is widely accepted within the forest industry, but it is also recognised that not all riparian zones in a catchment are equally effective in influencing catchment yields.

Since riparian soils are often the wettest and most fertile within a catchment, and are therefore extremely productive, there is strong interest in moving away from the use of a standard width throughout the catchment, and rather to identify the required limits to the riparian zones on the basis of more objective criteria. This need has led to the development of a classification system for riparian zones, in which three categories are defined on the basis of the presence and persistence of saturated soil and stream flow in the watercourse (Figure 1.1). Thus, type A zones are associated with ephemeral streams in the upper reaches of a watercourse, and are not associated with a permanent body of saturated soil. Type B riparian zones occur further downstream, and are characterized by ephemeral flow, and a fluctuating water table defining the surface of a permanent saturated soil water body. Type C riparian zones occur further down stream, and are characterized by permanent channel flow. Theoretical analyses of these different riparian zones have led to the conclusion that riparian vegetation alongside type A zones has minimal impact on catchment water yields, and therefore does not require exclusion status. Catchment yields are believed to be especially sensitive to vegetation influences along type B zones, since changes in plant water use can greatly alter the surface area of saturated soil, and hence the amount of saturation overland flow of that region of the stream. Type C riparian zones are characterized by perennial flow

and often less fluctuation in the surface area that generates saturation overland flow. Vegetation influences on catchment yield are believed to be less than for type B riparian conditions. The reader is referred to the practical field guide (Department of Forestry 2001) for a complete description of the procedures used to delineate riparian zones/wetlands in forestry plantation catchments.

This concept of the influence of riparian saturated zones in moderating land use impacts on catchment water yields potentially holds great significance to water conservation in forestry catchments, and the overall efficiency of water use by plantation forests. What is unclear is the size and significance of this moderating influence. The purpose of this research project is to investigate the links among vegetation, saturated zone dynamics, and runoff generation for the different classes of riparian zone, and to test the hypothesis that riparian zone vegetation has a significantly variable effect on catchment yields.

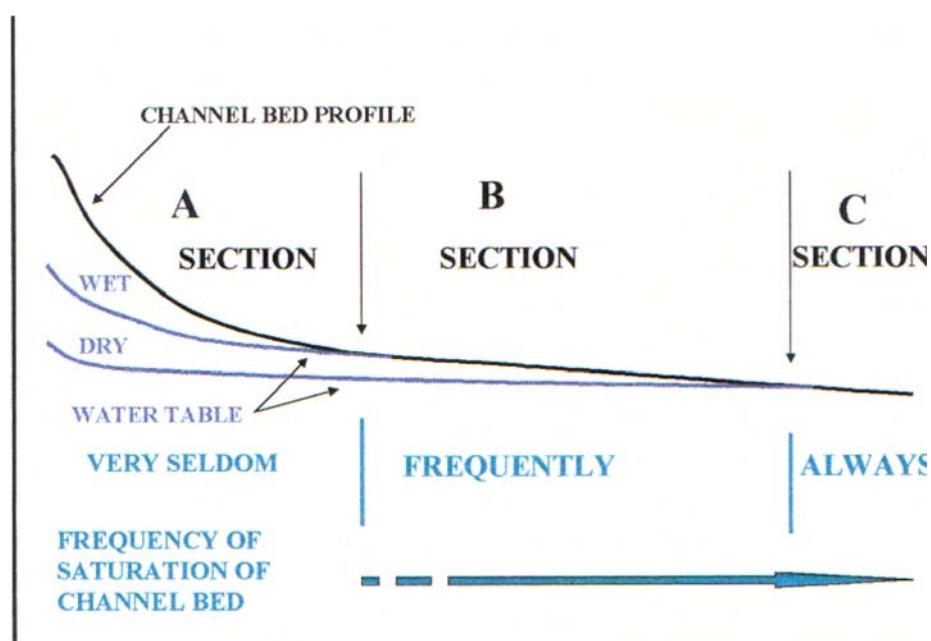


Figure 1.1. Longitudinal profile of a river bed showing classification of channel sections.

### Experimental Approach

Two approaches have been adopted in this study namely,

- 1 Hillslope soil water dynamics measured before and after a change to riparian or hillslope vegetation, to record the effects of the treatment on the soil and streamflow regime.
- 2 A modelling study to see the data from above in the context of the complete catchment. The streamflow models tested in this study are the Agricultural Research Catchment Unit (ACRU) and the Soil Water Assessment Tool (SWAT).

## CHAPTER 2

### The Study Area

The Mistley-Canema estate (Mondi Forests) in the Seven Oaks district is situated in the KwaZulu Natal midlands (Figure 2.1). The Bioresource Group (BRG) (Camp, 1997), is “moist midlands mistbelt”. The area is generally hilly, rolling country, with a high percentage (46%) of arable land. The climate is humid; with an annual rainfall ranging from 800 mm to 1280 mm. Heavy mists are a common and are an important feature, providing additional moisture, particularly to forests. The mean annual temperature is 17°C. Climate hazards include occasional droughts, usually of short duration, occasional hail and frost which vary from slight to severe. Hot “berg winds”, followed by cold fronts, make for unpredictable conditions, particularly in spring and early summer (Camp, 1997).

The natural vegetation of the area was previously *Themeda triandra* grassland. Only a few relic patches remain, as the high potential of the arable areas has meant that little value has been placed on the natural veld. The potential of the soils of the area are high, in spite of the fact that the inherent nutrient status is very low. Particular problems are P-fixation and Al-toxicity. The soils are highly leached and the area is suited to intensive farming systems. Forestry is ecologically suitable and is the most widespread land use, with gum (eucalyptus spp.), pine and wattle being the species of choice. Sugar cane is grown on sites where drainage of cold air is good, ensuring that no frost or only light frost occurs.



**Figure 2.1** The locality of the Seven Oaks district in the KwaZulu Natal midlands

## 2.1 Study Site

Two small catchments, planted with 13-year-old wattle were selected as the study site. The catchments are situated at the Mistley-Canema Estate (Mondi Forests) in the Seven Oaks district, approximately 70 km from Pietermaritzburg (30.67°S, 29.19°E). The catchment on the Mistley Estate at Seven Oaks has both types A and B class riparian zones (Figure 2.2).

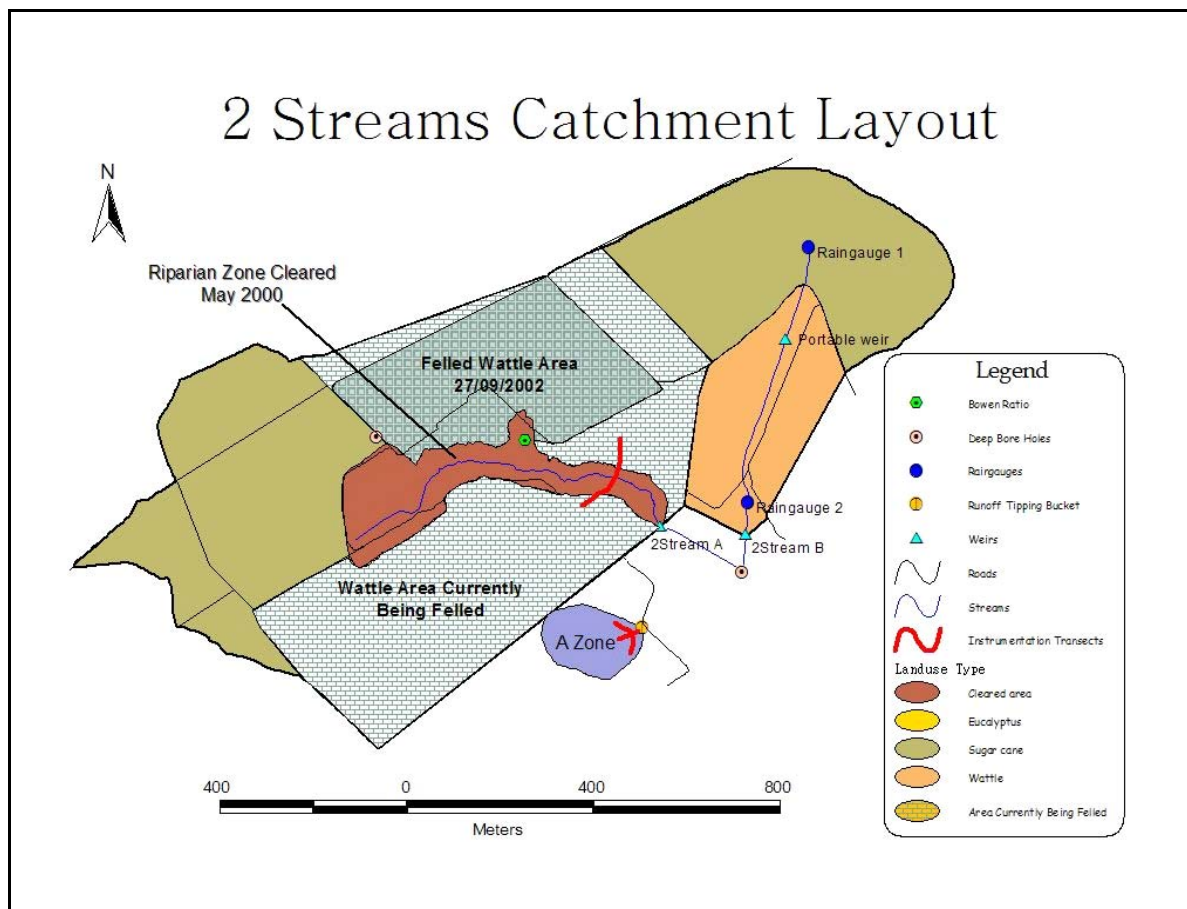


**Figure 2.2.** Map showing the position of the various monitoring stations on the North and South hillslope study transects together with the progress with the clearing of the *Acacia* trees.

The catchment details (boundaries, streams, roads, weirs, rain gauges, landuse, and monitoring sites) have been mapped using a Trimble geographical positioning system, with accuracy better than 0.20 m and captured into Arc View GIS coverages (figures 2.2 & 2.3). A profile of the monitoring transect for the B-zone was also created (Figure 2.4). The position of the riparian zone has been delineated using the new riparian classification that delineates according to the presence of both a permanent and temporary water table. The Two Streams catchment has been classified as a typical “B-stream”, where the contact of the water table and the stream is not permanent as in “C class” streams. A-zones were identified in the upper catchment where no water table exists.

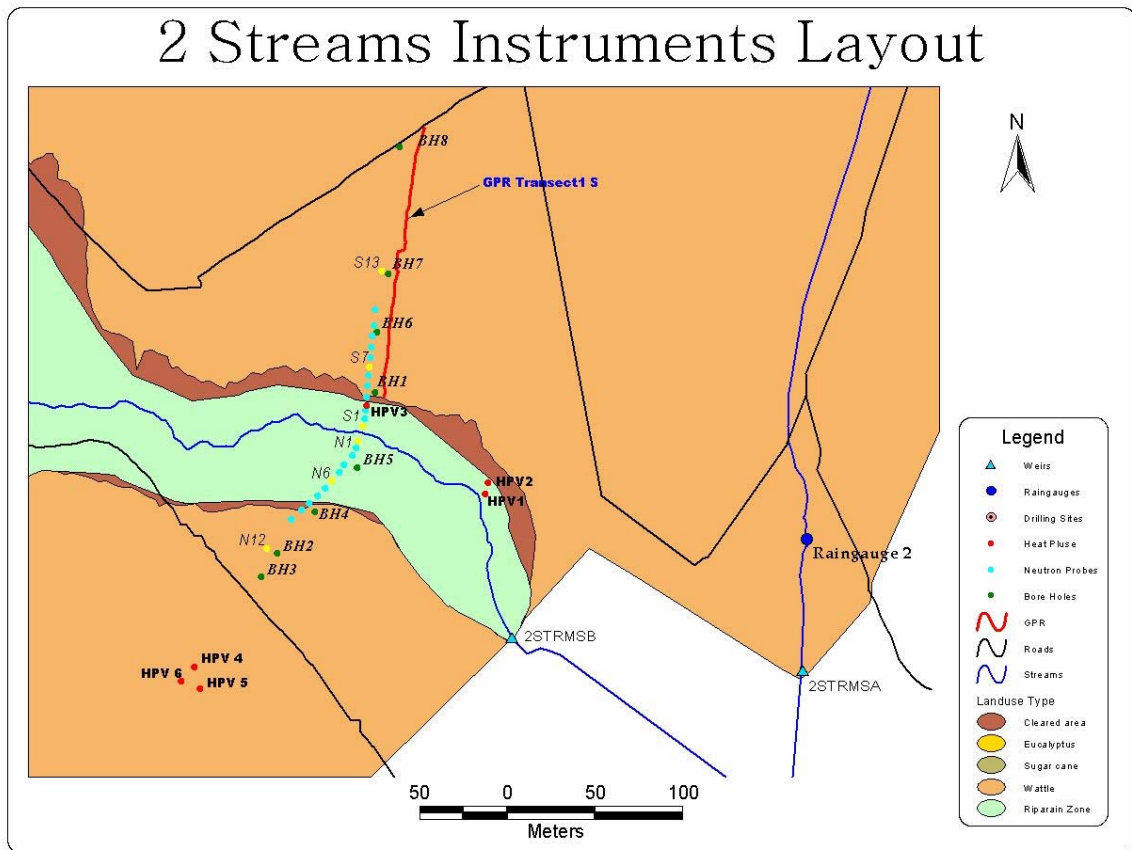


**Figure 2.3.** Map showing the position of the various monitoring stations on the North and South hillslope study transects.

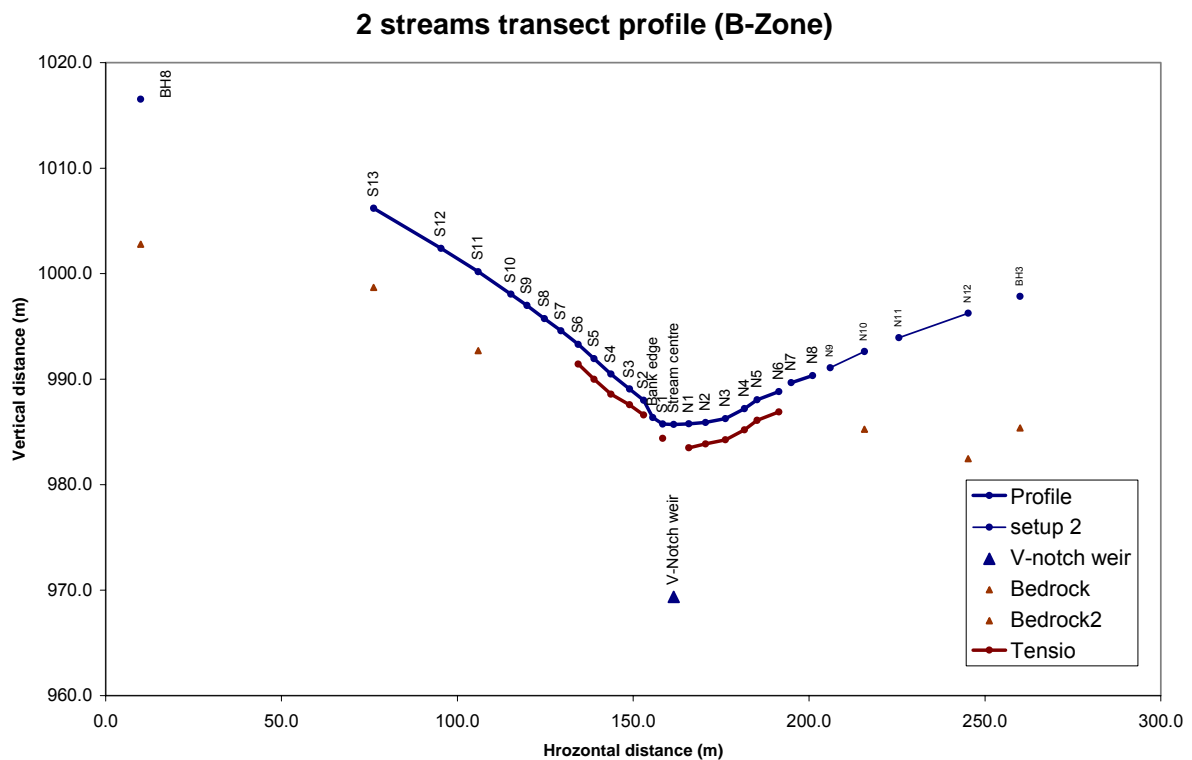


**Figure 2.4.** Transect profile of monitoring stations for the two streams catchment.

## **CHAPTER 3**

### **Methods and materials**

#### *3.1 Rainfall*

Rainfall is being monitored at three sites in the catchment area (see Figure 22 for location) using tipping bucket raingauges (MCS-160) with a 0.2 mm resolution. . The first site is located high up the catchment while the second is close to the main weir so as to gain insight into the distribution of rainfall within the area. In general there is good correlation between these two gauges. The experimental set-up includes an additional raingauge which is located within the plantation canopy in the A-zone site, but this has been used primarily to evaluate interception losses.

#### *3.2 General climatic variables*

A Campbell Scientific automatic weather station, located near the Mondri lookout tower, was used to measure ambient temperature, relative humidity, rainfall (0.1 mm), windspeed and direction at hourly intervals during the study.

#### *3.3 Streamflow*

The experimental framework consists of a V-notch weir built in the river of the catchment to be cleared. A second weir was established on an adjoining stream to act as a control. Streamflow has been monitored continuously in the main catchment using a 457.2 mm, 90° V-notch weir with a Belfort Streamflow recorder modified with an MCS 250-01 streamflow encoder. This was later replaced after theft of the original instruments with an Ott Streamflow recorder and pressure transducer supplied by DWAF. The calibration of the weir was carried out by DWAF staff.

#### *3.4 Ground Water Monitoring*

The Department of Water Affairs installed eight boreholes (drilled to bedrock) in February 2000. The boreholes are located along the soil water monitoring transects. Two deep boreholes (60 m +) have been drilled at the upper and lower reaches of the catchment to monitor the deep aquifer. Depth to the bedrock varied between approximately 6 m near the stream to 14 m at the top of the slope.

#### *3.5 Soil water dynamics*

Since February 2000 intensive soil water monitoring instrumentation networks, spanning the extent of the B-zone were established along a north-south aspect (Figure 2.3). Twenty-five aluminium access tubes were also installed to a depth of 2.0 m roughly equidistant apart along the transect (Figure 2) so that soil water content could be measured with a neutron probe. These measurements are made at six depth intervals.

Since soil water retention is an important parameter that regulates the storage and movement of water and ultimately plant growth, it was considered important to gain insight into this parameter as it relates to hillslope dynamics. Water at any given point in the soil can be associated with a specific energy state. This is influenced by gravity, the forces arising from the presence of solutes in the soil solution and the forces generated by the mutual attraction of

the soil water and the solid matrix. In practice it is difficult to evaluate each of these components separately. Because of this the total soil water potential is more easily obtained by measuring another related property or properties such as hydrostatic pressure, vapour pressure or elevation. A useful measure is the soil matric potential, which relates the soil water pressure against that of the atmosphere. In unsaturated soils the soil water pressure is sub-atmospheric due to capillary forces and hydration envelopes on the solid matrix. In saturated soils on the other hand, as would normally be the case beneath a water table, the pressure is positive.

To measure soil water potential, fifty-six tensiometers arranged in fourteen nests of four tensiometers each were installed at strategic locations along the common transect within the catchment (Figure 2). The four tensiometers within each nest, have been installed at roughly 0.3m, 0.6m, 0.9m and 1.8m depths. Briefly, each tensiometer comprises a porous ceramic cup connected to a de-aired water filled tube terminated on the upper end by a differential pressure transducer. The porous ceramic allows for the exchange of water between the tensiometer and the surrounding soil environment until a state of equilibrium is reached. The pressure transducer senses the difference between the ambient air pressure and the soil water pressure and emits a voltage signal that is recorded by a CR10X datalogger every 12 minutes. A calibration relationship, derived for each pressure transducer before the start of this study, allows for the conversion of the voltage signal to soil water pressure, which is then corrected for the depth of the ceramic below the soil surface.

A further fourteen nests of tensiometers were installed in a spatially distributed system within the A-Zone. Each nest has three instruments located at soil depths of approximately 0.3, 0.6 and 1.5 m. At six of these nests neutron probe access tubes were installed to soil depths approaching 6m. Measurements of water content at 0.30m depth intervals are made using the neutron probe. The drainage line in the A zone was further instrumented with a surface and subsurface runoff plot. A tipping bucket connected to a Hobo event logger measures the amount of surface runoff from the plot while rapid interflow is collected in specially designed buckets that also act as sediment traps.

For reasons expanded upon later in this report, five additional nests of watermark sensors manufactured by the Irritol Corporation were installed along a single transect within the A-Zone in October 2003 and this was extended into the B-Zone and riparian area during November 2004. These are sensors that contain electrical resistance circuitry embedded within a specially designed granulated matrix. Since the pore-size distribution of the matrix is known a measure of water potential is obtained from the soil water content which in turn is related to electrical resistance. The manufacturer offers a calibration relationship between electrical resistance and soil water potential. Whereas tensiometers cease operating beyond a matric potential of -80 to -90 kPa, watermark sensors have a far greater operating range, typically in the order of 0 to -200 kPa, although for drier conditions these sensors would need to have their calibration verified. Watermark sensors are, however, temperature dependent so soil temperature, which is considered in the calibration relationship, needs to be measured. All sensors were mounted at the end of a 25mm PVC conduit within which was added a copper-constantan thermocouple to obtain a measure of soil temperature. To install the sensors a 30 mm in diameter shaft was first augured to the required sensor depth. A weak slurry containing the recently excavated soil was then poured down the shaft before installing the sensor. This was necessary to minimise the risk of airgaps, between the sensor and surrounding soil. All sensors were wired via an AM416 Campbell multiplexer to a CR10X datalogger programmed to record soil water potential every 12 minutes. The advantage of this system, beyond that of a greater operating range, is that once installed, unlike tensiometers, no further maintenance of the sensors is required.

Undisturbed soil cores, retained within a 50mm x 75mm stainless steel sleeve, were collected from the B and riparian zone in order to measure their water retention properties, bulk density and saturated hydraulic conductivity. Three depths (0, 0.50m and 1.5m) were sampled in the B-Zone and two depths (0 and 0.50 m) in the riparian zone. An equivalent set of disturbed samples were collected for the measurement of particle size, pH and organic carbon. Water retention and saturated hydraulic conductivity were measured on the same cores. This meant that the bulk density of each core had to be determined beforehand as any loss of soil when measuring the saturated hydraulic conductivity, could compromise the accuracy of the results. Considering that the mass of the stainless steel sleeve used to retain the sample was known, only the field mass water content of each core needed to be determined in order to calculate its equivalent oven-dry mass and thus its bulk density. This measurement was carried out on the excess soil removed during the trimming of each core. The cores were saturated overnight and equilibrated at matric potentials of 0, -1, -2, -3, -4, -5, -6, -8, -10 kPa using sand bath tension tables and at -30, -60 and -100 kPa using pressure plate apparatus.

After equilibration at a matric potential of -100 kPa, the steel sleeve containing the sample was lengthened, by taping an empty duplicate sleeve to the upper end. The cores were then re-saturated overnight and fitted with a plastic funnel that contained a wire mesh upon which the base of the sample rested. Saturated hydraulic conductivity was measured by the constant head method (Klute and Dirksen 1986) with a hydraulic head of 50 mm.

The bulk density ( $\rho_b$ ) and the mass water content of the sample ( $\theta_m$ ) at each matric potential were used to calculate the volumetric water content ( $\theta_v$ ) using the relationship  $\theta_v = \theta_m \times \rho_b / \rho_w$  (where  $\rho_w$  = density of water). During trimming of the cores a portion of the excess soil was air-dried, crushed to pass a 2mm sieve, and poured into pre-weighed rubber rings (9.5 mm high, 52 mm i.d.). The samples were levelled within the rings, capillary saturated for 24 h and desorbed on a 15 bar pressure plate at a matric potential of -1500 kPa. After reaching equilibrium the content from each ring was removed and its mass water content determined by oven drying. This mass water content and the bulk density of the core from which the sample was obtained was used to make the conversion to volumetric water content. This procedure was used to reduce the time that would have been required to equilibrate the large cores at -1500 kPa matric potential. Readily available water (RAW) and plant available water (PAW) were calculated for each treatment as the amount of water retained between matric potentials of -10 and -100 kPa and -10 and -1500 kPa respectively (Smith et al. 1995).

The water retention data were fitted by the van Genuchten (1980) (VG) model,  $\theta = \theta_r + (\theta_s - \theta_r) [1 + (\alpha \cdot h)^n]^{-m}$ , where  $\theta$  is the actual volumetric water content,  $\theta_s$  is the saturated water content,  $\theta_r$  is the residual water content usually taken as the water content at the wilting point (-1500 kPa),  $h$  is the water potential,  $\alpha$  is a curve fitting parameter, the inverse of which relates to the air entry potential, and  $m$  and  $n$  are dimensionless parameters related to the pore size distribution (van den Bergh *et al.* 1997). It has been suggested by van Genuchten (1980) that the parameter  $m$  may be evaluated by the relationship  $m = 1 - 1/n$ , which reduces the number of parameters that must be determined from five to four. Beginning with the measured water retention curve and an initial estimate of the parameters, a non-linear least squares approach was used to iteratively find an equation that maximized the sum of squares associated with the model while minimizing the residual sum of squares. The residual sum of squares represents the degree of bias or lack of fit and the contribution of random errors. In this study the RETC code (van Genuchten *et al.* 1991) was used to parameterise the mean water retention curve determined from four replicates.

### 3.6 Evaporation Monitoring

Direct measurements of sapflow by trees were measured using the heat pulse velocity technique. Evaporation of the recolonised natural grassland in the cleared riparian strip has been monitored using the Bowen ratio energy balance technique.

#### 3.6.1 A description of the heat pulse velocity technique

##### 3.6.1.1 Theory of the heat pulse velocity technique

The heat pulse velocity (HPV) technique measures the velocity of a heat pulse propagating through a tree using the compensation technique (Huber and Schmidt, 1937; Swanson, 1974 cited by Dye *et al.*, 1992). The temperature rise in the thermistor probe as a result of the application of a heat pulse is measured at a distance  $X_u$  upstream and  $X_d$  downstream from the heater probe. According to Swanson (1983) (cited by Olbrich, 1994), the velocity of the heat pulse ( $u$  in  $\text{m s}^{-1}$ ) is calculated as:

$$u = \frac{(X_u + X_d)}{2t} \quad 2.17$$

where  $t$  (in second) is the time it takes for the temperature at  $X_u$  and  $X_d$  to become equal (Dye *et al.*, 1992) or for the Wheatstone bridge voltage to return to the initial balance point after the heater is pulsed (Olbrich, 1994), where  $(X_u + X_d)/2$  refers to the probe separation (Olbrich, 1994). Both  $X_u$  and  $X_d$  are regarded as positive quantities.

The heat pulse velocity is corrected for wound size or width according to Swanson and Whitfield (1981):

$$u' = p + qu + ru^2 \quad 2.18$$

where  $p$ ,  $q$  and  $r$  are correction coefficients derived for the wound size, diameter of Teflon probes (thermistor probes) and probe separation distance.

Finally, the sap flow ( $v$ ), is calculated from the corrected heat pulse velocity ( $u'$ ) (Marshall, 1958):

$$v = \rho_b (m_c + c_{dw}) u' \quad 2.19$$

where  $\rho_b$  is the dry wood density ( $\text{kg m}^{-3}$ ),  $m_c$  the fractional water content of the sapwood on a dry weight basis (unitless), and  $c_{dw}$  the specific heat capacity of dry wood ( $0.33 \text{ J kg}^{-1} \text{ }^\circ\text{C}^{-1}$ ) (Dunlap, 1912 cited by Dye *et al.*, 1992).

The various sap fluxes ( $v$ ) measured at different depths below the bark of a tree, are regarded as representative of a ring of sapwood centred at the probe depth. The total sap flux per tree is therefore calculated as the sum of the partial areas (a concentric ring area with limits midway between successive thermistors) multiplied by their associated sap fluxes. The sap flux per tree can be converted into sap flux per unit area, using the tree espacement.

The wound size for each set of probes is measured at the end of the experiment. The sections of the tree trunk containing the probe implantation holes are cut out. Then each block

containing the probe implant holes is cut longitudinally at the depth at which the thermistors were implanted. The area is then shaved smoothly with a microtome after which the wound width is identified by discolourization, and measured to the nearest 0.1 mm. Measurements are taken midway between the position of the heater probe and the two thermistor probes. From these measurements, the average wound width is calculated for each tree. The assumption is generally that the same wound size existed for the duration of the experiment. The wood density is also calculated at the end of the experiment, using a fresh sample of sapwood.

### 3.6.1.2 The heat pulse velocity equipment

The heat pulse velocity system consisted of a datalogger) and a set of probes consisting of two thermistor probes and one heater probe.

Teflon probes, each with a thermistor imbedded, are connected in a Wheatstone bridge configuration by using the datalogger. A heat pulse is generated when a current is supplied for 0.5 to 1 s to the heater probes. The data recorder then estimates the time it takes for the bridge to return to the initial balance point, following the heat pulse.

### 3.6.1.3 Patching of heat pulse velocity data

Tree transpiration data loss during a field experiment can result from low battery voltages, corrosion of heater probes, and cracks around heater and thermistor probes and subsequent large wound widths.

Dye *et al.* (2001) found good agreement between daily sapflow (total transpiration) measured with the HPV technique and the product of the average daily water vapour pressure deficits  $e_s - e$  and the daylight hours, for a number of tree species. This relationship has been used by Dye *et al.* (2001) to accurately patch missing sap flow data.

### 3.6.1.4 Application of the heat pulse velocity technique for measurement of *A. mearnsii* tree transpiration

The heat pulse velocity technique (Huber and Schmidt, 1937; Swanson, 1974 cited by Dye *et al.*, 1992) was used to calculate the transpiration (sapflux) of trees within the riparian zone and upslope sites. Four 12-channel heat pulse dataloggers (custom made) were used to measure the velocity at which a heat pulse moves through a tree stem at different depths below the cambium. Measurements were made at hourly intervals. Swanson (1983) found that radial differences in the sapflux occur, and suggested that sets of probes be implanted to different depths within the sapwood (e.g. d1 to d4) (Fig. 5.6). Four sets of probes (a set consisting of a heater probe and two thermistor probes) were therefore installed at different depths (9, 14, 21, 28 mm) below the cambium of each *A. mearnsii* tree studied. This ensured that the variation in sapflux over the sapwood was covered and reflected in the tree transpiration measured.

As the accuracy of the sapflux measurements and heat pulse velocity depends on the distance between the probes, a drill jig with three aligned holes was used to install the probes accurately and parallel to each other. The heater probe was installed in the centre hole, and the two thermistor probes were installed at 5 mm below and 10 mm above the heater probe (Fig. 3.2).

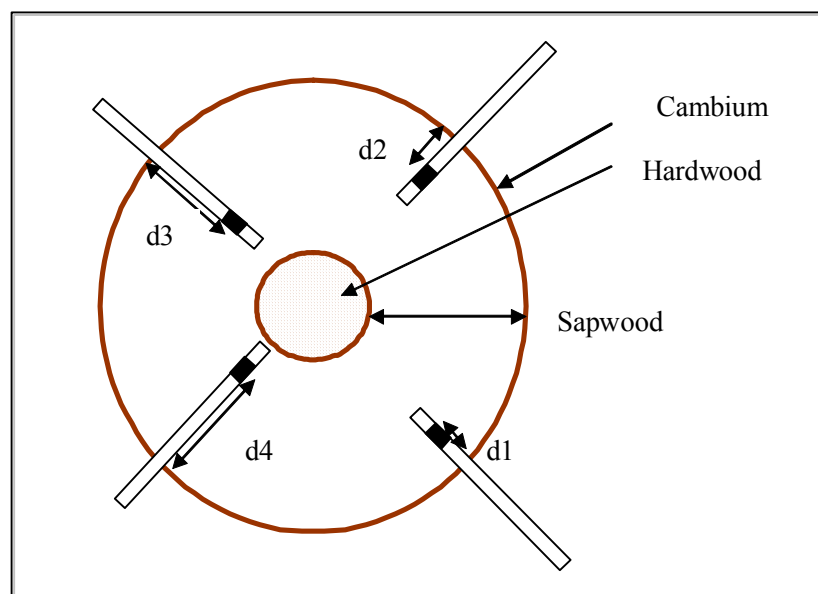


Fig. 3.2 Schematic of the implantation of sets of probes at different depths below the cambium, into the stem of an *A. mearnsii* tree

### 3.6.2 Bowen ratio energy balance technique

#### 3.6.2.1 Theory

The Bowen Ratio Energy Balance technique estimates the components of the energy balance and therefore the total evaporation above a surface.

The simplified energy balance (Eq. 1) above a surface is given by :

$$R_n - G = \lambda E + H \quad 1$$

where  $R_n$  is the net irradiance,  $G$  soil heat flux density,  $\lambda E$  latent heat flux density and  $H$  sensible heat flux density, all in  $\text{Wm}^{-2}$ . Solution of equation 1, requires the measurement of the available energy flux density ( $R_n - G$ ) and the air temperature and water vapour pressure profile differences above a surface. The available energy flux density at a surface is partitioned into latent heat flux density (energy driving evaporation), and sensible heat flux density (energy heating the air). The latent heat flux density is a function of the water vapour pressure profile difference and the sensible heat flux density a function of the air temperature profile difference.

### 3.6.2.2 Instrumentation

The various components of the energy balance were measured with a 023 A Bowen ratio energy balance system (Campbell Scientific, Inc.). The net irradiance is measured with a net radiometer, installed above the vegetation (Figure 3.1). The soil heat flux density in the upper 80 mm depth of soil was calculated from the average soil temperature and soil water content over 80 mm, and the average soil heat flux at 80 mm. Two Bowen ratio arms with air temperature sensors and air intakes for water vapour pressure measurements were installed above the plant canopy. The lower arm was installed at least 1 m above the vegetation surface with the separation distance between the arms of approximately 1 m. The air temperature profile difference was calculated from the air temperatures measured with fine wire, type-E thermocouples (resolution 0.006°C) located at the end of each Bowen ratio arm. The water vapour pressure difference between the arms was calculated from water vapour pressure measured with a dew-10 hygrometer (resolution 0.01 kPa), *via* air intakes situated at the end of each Bowen ratio arm.

The required measurements were performed with CR23X datalogger installed in the riparian zone. Measurement intervals were 1 s for the air temperature and water vapour pressure profile differences, and 10 s for the net irradiance, soil heat flux and temperature and soil water content. These frequent measurements were subsequently averaged or totalled over 20 minute periods and output to a storage module.

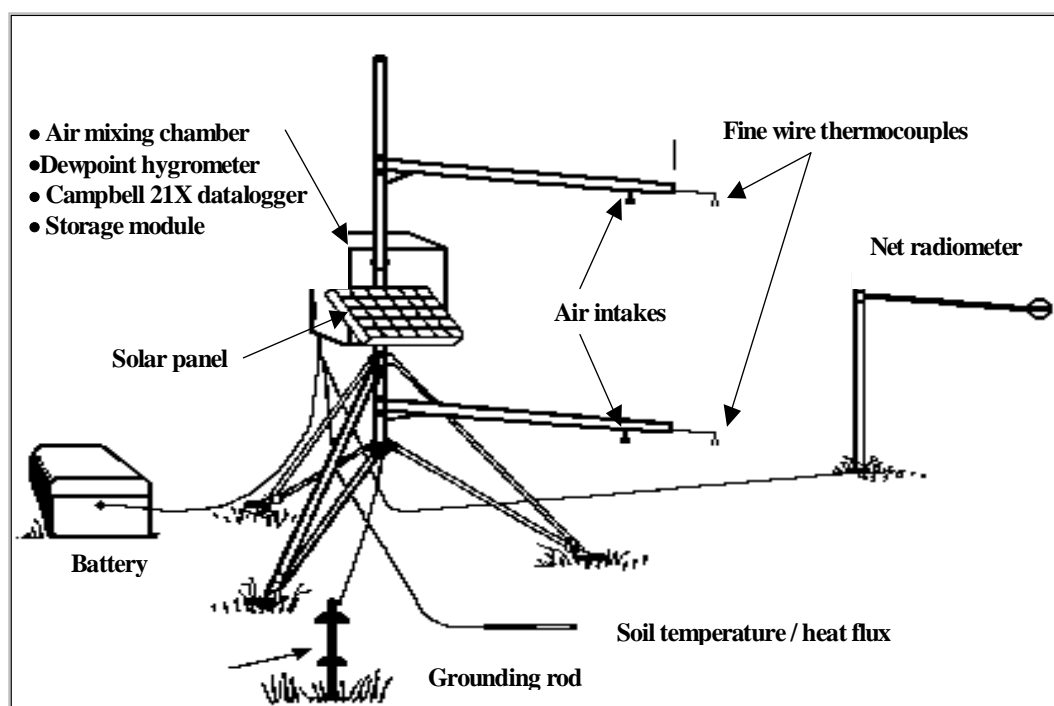


**Figure 3.1 A diagrammatic representation of the Bowen ratio system**

### 3.6.2.3 Installation of Bowen Ratio Energy Balance equipment

The Bowen ratio sampling arms and net radiometer were mounted onto a 6 m mast. The sampling arms of the Bowen Ratio Energy Balance system were orientated due north/south to avoid partial shading of the thermocouples on the arms, while the net radiometer was positioned north/south to prevent sensor shading. The air sensed by sensors mounted on

these arms was representative of the surface studied. The lower arm was installed low enough that the bulk vegetation surface environment was not sensed, whereas the upper arms were installed low enough not to sense a different environment upwind. In order to ensure that the air temperature and water vapour profile differences measured were within the resolution of the sensors, a separation distance of at least 1 m between the Bowen ratio sampling arms was maintained, with the height of the lower Bowen ratio arms at approximately 1 m above the vegetation.

As the moist upland grassland surface was uniform, the surface soil heat flux density was estimated using a single pair of soil heat flux plates and two pairs of averaging thermocouples. The soil heat flux plates were installed at 80 mm below the soil surface, the averaging thermocouples at 20 mm and 60 mm below the surface, and the soil water content reflectometer within the upper 80 mm of soil.

### 3.7 Geo- Physical survey: Ground Penetrating Radar

#### 3.7.1 Mapping the bedrock profile

Ground-penetrating radar (GPR) is a well-established technique that has been used over the past few decades to evaluate soil properties and to estimate the variability and the composition of the soil affecting many disciplines such as agriculture, environmental, construction, and mining engineering.

The objective of the study was to obtain the bedrock profile of the Two Streams study site. This information was considered important for understanding the hydrology within the vadose zone.

#### Theory:

Ground penetrating radar is a fast and efficient field technique that can be used to construct continuous bottom profiles of the underlying bedrock within catchments. The GPR consists of a transmitting and receiving antennae linked by a cable to the control and recording units. The transmitter radiates a short pulse of electromagnetic energy into the ground. When the signal meets a change in the electrical properties of the soil, part of that signal is reflected. Then, the receiver detects it after amplification. The radar penetration to a reflective interface is measured by the travel time between the transmission and reception of the reflected waves. This two way travel time is converted to a penetration depth from the relationship:

$$d = ct/2 \sqrt{\epsilon}$$

Where  $d$  : depth to the interface (m)

$c$  : propagation velocity of electromagnetic waves in a vacuum,  $c = 3 \times 10^8$  m/s

$t$  : two way transmitter-receiver travel time of the reflected waves (s)

$\epsilon$  : dielectric constant relative to a vacuum

There is a compromise between the range and the resolution for a GPR system : lower frequencies have an increased penetration but reduced resolution capabilities compared to higher frequencies. Radar systems with a frequency of 100MHz have been shown to have the best range resolution compromise in many geological environments (David and Annan 1989). In addition, as the conductivity of soil increases with moisture content, soils with a high moisture content rapidly absorb the electromagnetic pulses, and restrict the effective probing depth of the GPR.

#### Equipment:

The radar system used was the Subsurface Interface Radar (SIR) System- 3 (Geophysical Survey Systems, Inc.).

It consisted of :

- A profiling recorder (model PR 8300) coupled with a DC amplifier.
- A 300Mhz antenna (transmitter – receiver, model 3105)
- A 120MHz antenna (transceiver, model 3110)
- A battery 12 V, 115A
- An antenna-recorder wire (30 m)
- A battery-recorder wire
- Extra paper and stylus.

Set-up:

- **Upper Control Panel :**

Print polarity : +/- (print positive and negative signal full).

Paper take-up : AUTO

{ Lines/inch : 100 (sets a scan line density of 100 lines per inches).  
Scan/sec : 16 (selects a graphic recording and radar scan speed of 16 scans/second). 32 scan/sec is too quick and 8 gives an image not dense enough.

Gain (surface, centre, deep) : fully counter clockwise to enable the automatic gain setting function.

Range : vertical scale, a 100 ns scale seems to be the most efficient. It depends on how deep you want to go. It's a compromise between depth and quality of image.

- **Lower control panel:**

Range: multiplies 3 digit range by 1 (1000) or 0.1 (100). Example: to have a 500ns range, set the upper control panel range to 500 and the lower control panel to 1000. To have 50, just switch the previous setting to 100.

Coupling: DC

Marke : SHORT or FULL, for an horizontal scale.

Scale lines: ON (vertical scale)

Threshold: "4 o'clock", clockwise raise threshold to eliminate low level (for a clearer sample).

Filters High pass: 10 cycles /scan

Low pass: 50 cycles /scan

Signal position: MANUAL

Phase: UP

XMIT rate: 50 KHz

Mode: RADAR

Clock: INT

Transects:

The study was performed at the Two streams project site.

Two transects were studied:

- South aspect transect: from Bore Hole number 8 on top (0m) to the stream (155m).
- North aspect transect: from Bore Hole number 3 on top (0m) to the stream (100m).

The north transect (from 0m to 135m) was recorded with a GPS and plotted using GIS.

Determination of the dielectric constant:

The dielectric constant is a property that depends of the kind of soil (moisture, composition, etc) and is required for accurately determining the depth of objects in the profile. For an average forested soil (pastoral land Hilly, Forested), the dielectric constant is 13 (Geophysical Survey System, Inc). Examples of dielectric constants of various materials (Geophysical Survey System, Inc) are given below:

Air	1
Fresh water	81
Sand (dry)	4 – 6

Sand (saturated)	30
Silt (saturated)	10
Clay (saturated)	8 – 12
Dry sandy coastal land	10
Marshy Forested Flat Land	12
Rich Agricultural Land	15
Pastoral Land Hilly, Forested	13

Nevertheless, it was considered necessary to try and determine the dielectric constant for the soil at Two Streams. We buried a metal tube (20cm long and 10cm diameter) 70cm deep in the soil. Several transects were made with the radar, using different ranges and antennas.

- 300 MHz, range = 50 ns (x2)
- 300 MHz, range = 25 ns
- 120MHz, range = 50 ns (x3)

Unfortunately, despite these attempts, no clear reflection was found to specify the location of the metal tube, and the specific constant could therefore not be determined.

Measurements:

- 13/07/00

Southerly aspect transect from 0m to 135m: 120 MHz antenna, range = 500 ns.

Northerly aspect transect from 0m to 75m: 120 MHz antenna, range = 500 ns

- 03/08/00

Southerly aspect transect from 130m to 155m: 120 MHz antenna, range= 500 ns and 100 ns.

Northerly aspect transect from 60m to 100 m: 120 MHz antenna, range = 100 ns

### *3.8 Site Management*

Following a short calibration period, all the trees in the “B” riparian zone were cleared in July 2000. Three seasons have since been monitored to assess the impact of this clear felling on runoff. The trees in the entire catchment were scheduled to be removed in April 2002 by Mondi but due to operational setbacks this was rescheduled for September 2002. The northern portion of the catchment was cleared, but due to difficulties with stripping of the bark this operation was stopped by Mondi. The final clearing of the B section of the catchment was completed in April 2004. The A section was cleared in August 2004. The project team and Mondi also agreed to leave the catchment fallow for a year following the completion of the clearing. This was to allow for the extension of the calibration period which was interrupted due to forestry management influences.

# CHAPTER 4

## Results and Discussion

### 4.1 Rainfall monitoring

A good set of rainfall records have been were collected since the start of this study. Daily rainfall totals are represented in Figure 4.1, and monthly totals are shown in Figure 4.2. Annual rainfall for the period June 2003 to May 2004 was 704 mm. This compares with 1018, 858, 934 and 904 mm for the 1999/2000, 2000/2001, 2001/2002 and 2002/2003 seasons respectively. The 2003/2004 reporting period was therefore characterised by dry conditions as the long term average for the area is 840 mm. These reflect the severe drought conditions experienced in KwaZulu Natal in the 2003/2004 season. The daily distribution of rainfall reflected these dry conditions with only a few rainfall events of over 30 mm recorded. By contrast the 2004/2005 data show that the recent rain events between July and December 2004 are higher than any previously measured rain events for the study period. The highest single rainfall event during this study was measured on the 19<sup>th</sup> of November 2004 when over 90 mm of rain fell.

Precipitation from the raingauge placed in the A-zone under the canopy was compared with a gauge in the open (2 steams II) to obtain an estimate of the interception losses in the wattle trees. These data showed that between March and June the direct interception loss to the canopy was in the order of 30%. Stem flow was not measured and the data was from a single raingauge. These the results should therefore be treated with caution. However, the data do suggest that interception losses during drought periods may be higher than expected, since interception losses are generally considered to be about 7% of the total rainfall.

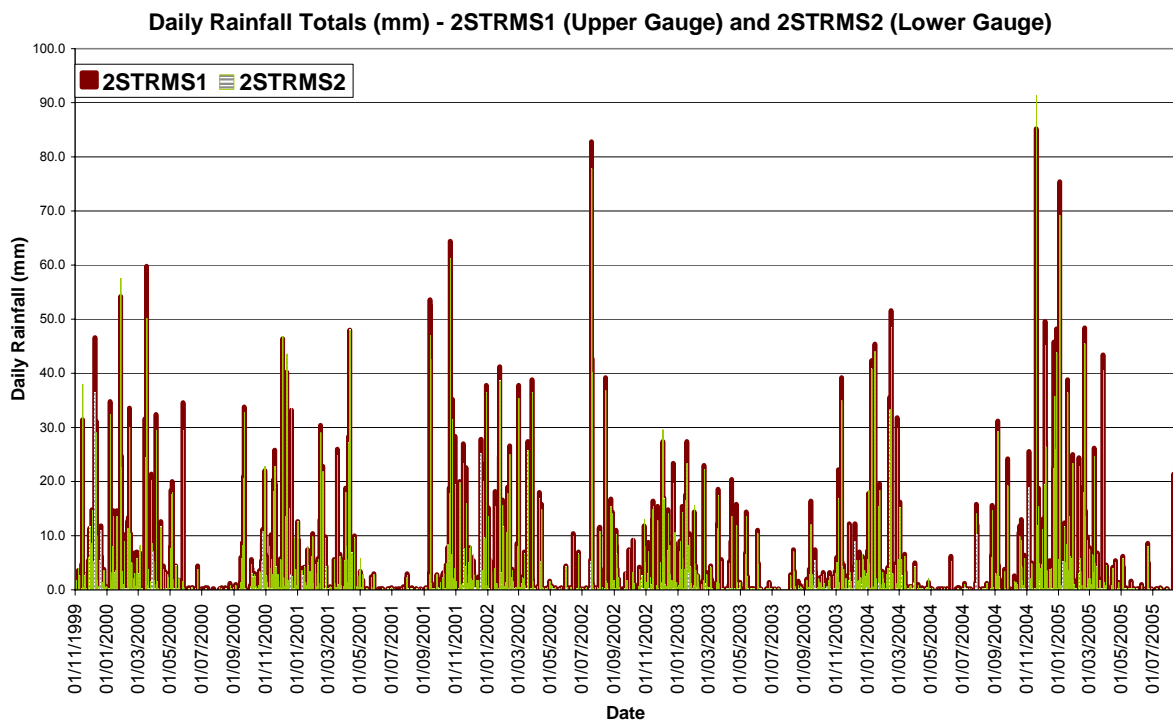


**Figure 4.1** Daily rainfall totals for the two automatic rain gauges at the Two Streams study site (November 1999 to July 2005)

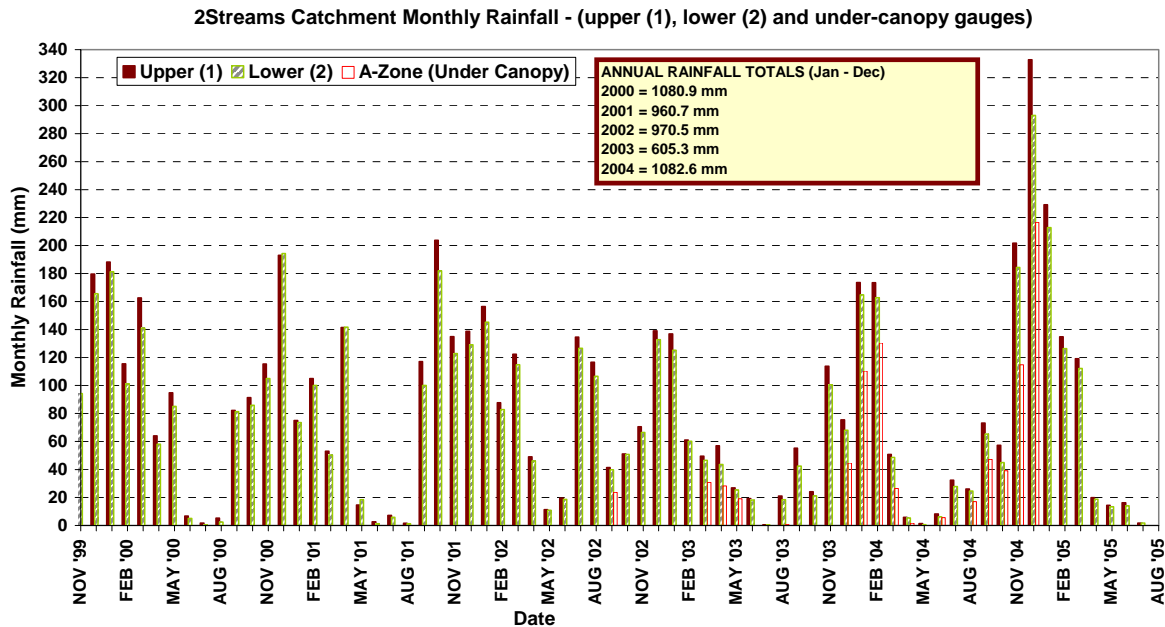


**Figure 4.2.** Monthly rainfall totals for the two automatic rain gauges at the Two Streams study site (November 1999 to August 2005).

#### 4.2 Streamflow gauging

Daily streamflow totals for the weir in the treated catchment (2STRMSA) together with corresponding rainfall data are illustrated in Figure 4.3, with cumulative streamflow and daily rainfall data represented in Figure 4.4.

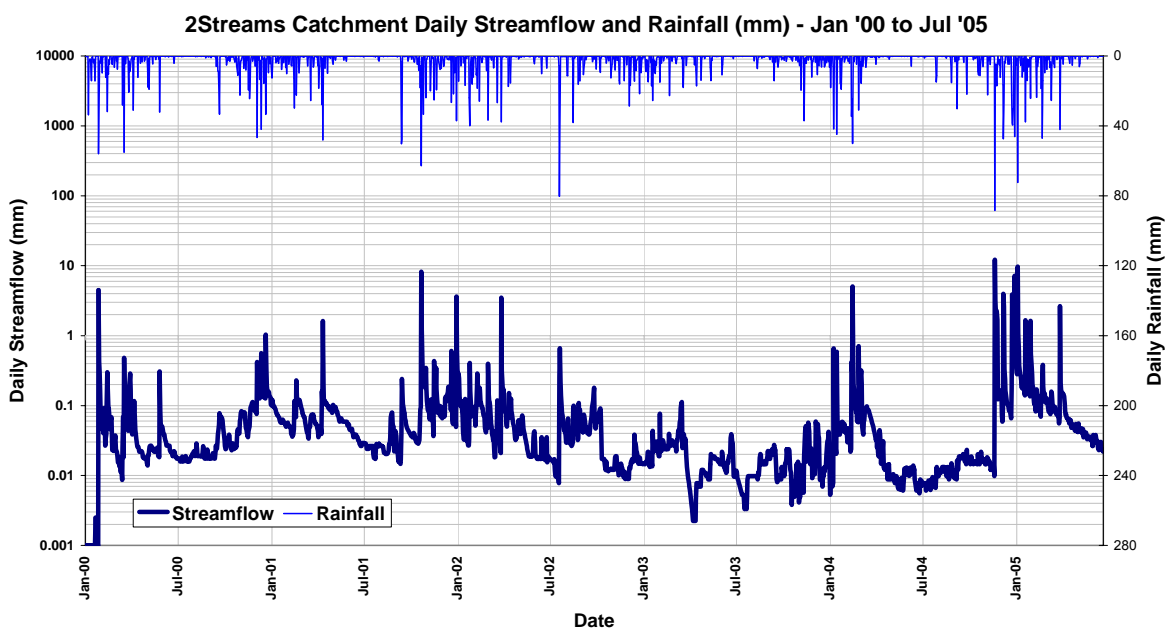


**Figure 4.3.** Daily streamflow totals (mm) with corresponding daily rainfall data (mm) for the treated catchment (January 2000 – July 2005).

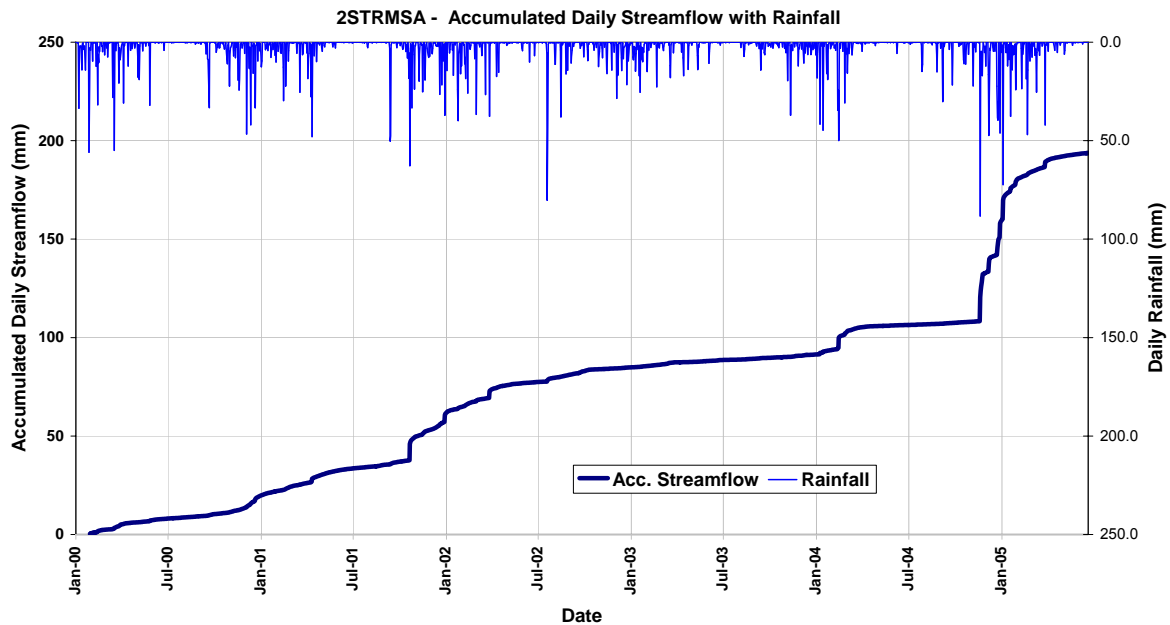


**Figure 4.4.** Accumulated daily streamflow totals (mm) with corresponding rainfall data for the treated catchment (January 2000 – December 2004).

Note that streamflow totals are plotted on a log scale in order to accentuate the lower flows. The removal of the 7.5 ha of trees from the delineated riparian zone in May 2000 clearly had a positive impact on the runoff from the treated catchment. Noticeable was the fact that the stream has continued to flow throughout the three winter periods of the study. This contrasts with the pre-riparian tree removal treatment when the stream only began flowing in late summer. The accumulated streamflow showed a decrease in runoff in the 2002/2003 season when compared with the previous years, a result of the low rainfall in the latter part of the 2002/2003 season. The daily streamflow in May and August 2003 reached its lowest level since February 2000 (Figure 5).

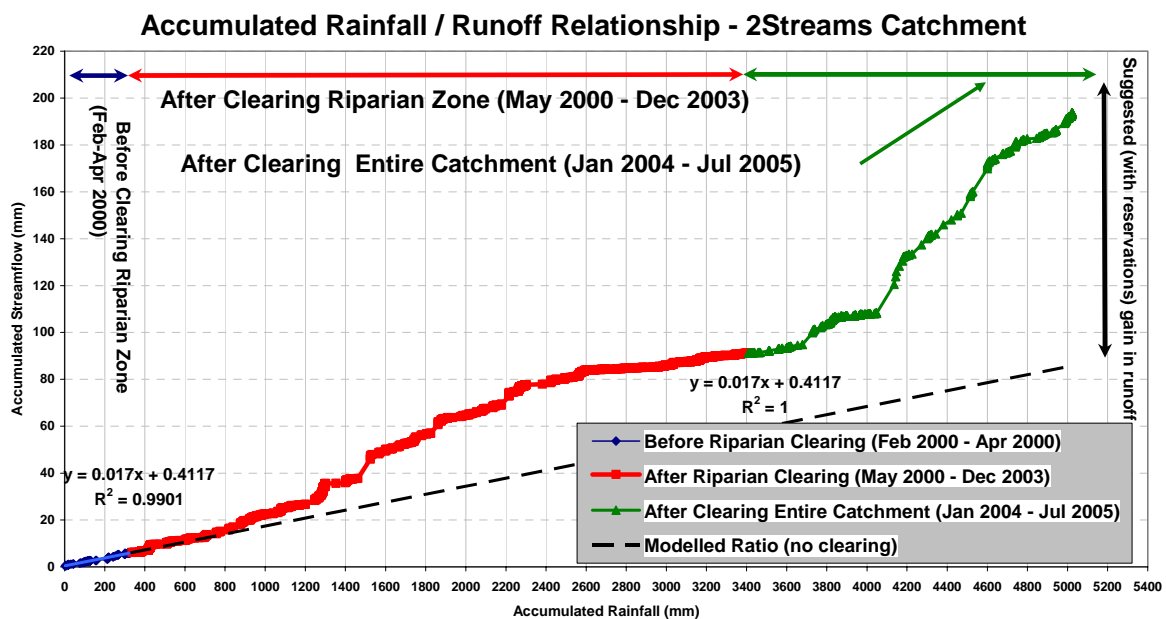


**Figure 4.5** The relationship between accumulated rainfall and accumulated streamflow for the Two Streams catchment A, for the period November 1999 to July 2005.

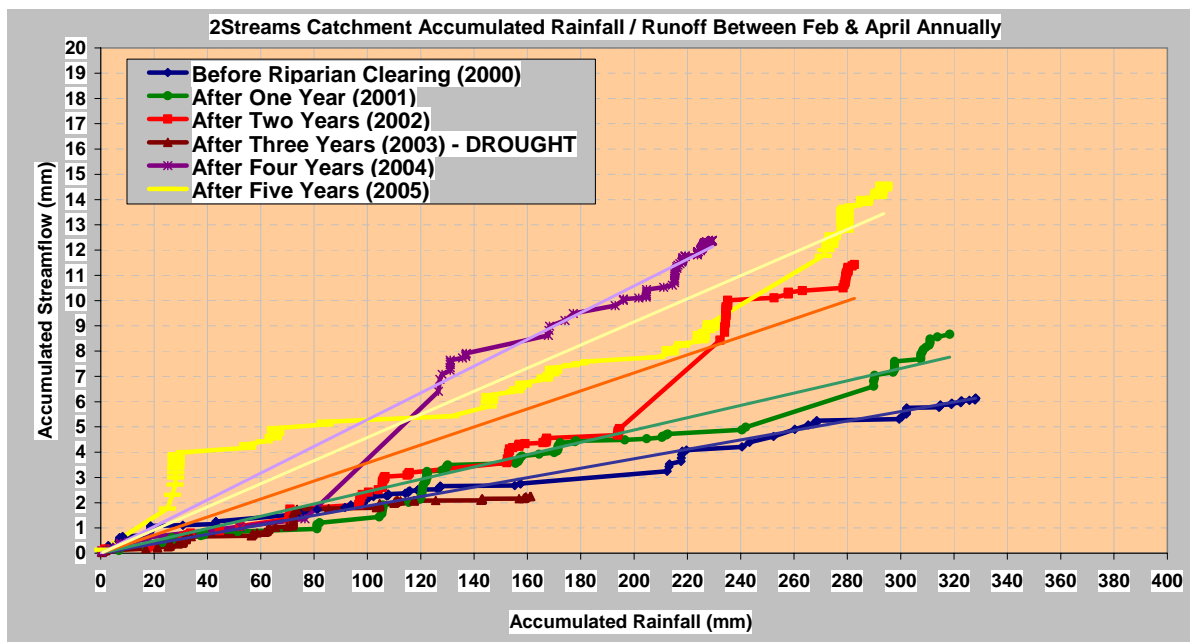


**Figure 4.6** The annual trends in the rainfall runoff relationship Two Streams catchment A.

The clearing of 14 ha of upslope wattle trees from the northern slope of the catchment in September 2002 did not appear to have any noticeable impact on streamflow, demonstrating the importance of the riparian zone for streamflow generation. However the clearing the entire catchment by December 2003 appears to have resulted a positive increase in the water yield from the catchment, despite the serious drought experienced in 2003/2004. The impact of the good rains in the 2004 season resulted in the streamflow reaching the highest levels recorded since the start of the experiment in 2000. Trend lines fitted to each year individually show the impacts of the different clearings. For example, if one considers the effect of 200 mm of accumulated rainfall then the impact of the riparian clearing is evidenced by a 1 mm increase in streamflow in 2001 and 3 mm in 2002. The drought and recovery of vegetation in the riparian zone brought the streamflow back to pre-treatment levels (year 2003). With the removal of trees in 2003/2004 the runoff is 10 mm; a 6 mm increase in the stream response over the 2000 steamflow of 4 mm. These data indicate that the combined removal of the wattle trees from the riparian zone and upslope sites has resulted in a 60% increase in the runoff from the catchment.

### 4.3 Soil Water Monitoring

#### 4.3.1 Soil Properties

The topsoil within the B zone has a sandy clay loam texture and is of the Hutton form (orthic A/ red apedal B). The bulk density is moderately low owing to the inclusion of plant litter that accumulates beneath the plantation canopy. This litter also leads to a moderately high organic carbon content of 5.9%. The movement of clay down the soil profile, termed clay illuviation, is a process often encountered in several of the deep well-drained red soils that are common within this region. Table 4.1 provides clear evidence of this process as the clay content at a depth of 1.5m was approximately 10% higher than that of the topsoil. Soil bulk density also increased with depth but remains within the range normally encountered in uncompacted soils of this type.

**Table 4.1** Soil physical properties at the two streams study site.

Position	Depth (m)	Sand (%)			Silt (%)			Clay (%)	Bulk Density (g cm <sup>-3</sup> )	HC (mm hr <sup>-1</sup> )	Organic Carbon (%)
		Coarse	Medium	Fine	Coarse	Fine	Very Fine				
B Zone North facing slope	Surface	3.8	18.1	22.6	7.2	15.2	8.6	24.6	1.14	94.2	5.9
	0.5	3.8	17.7	20.9	6.5	12.7	7.7	30.8	1.21	127.2	3.7
	1.5	5.1	14.1	19.0	6.0	10.2	8.8	37.0	1.25	132.7	0.9
Riparian zone	Surface	0.5	1.7	4.1	18.7	36.5	9.6	29.0	0.85	150.7	12.6
	0.5	3.8	9.9	18.4	15.9	23.8	18.4	10.0	1.09	172.2	7.7

Sediment that is carried in suspension from further upstream is deposited within the stream bed and along the stream verge as fine silt. This particle size class is therefore the dominant fraction of the soil in the riparian zone leading to a silty clay loam texture. Alluvial soils are often unconsolidated which accounts for its low bulk density of 0.85g cm<sup>-3</sup> and high saturated hydraulic conductivity. The organic carbon, namely 12.6% in the topsoil and 7.7% in the subsoil is also extremely high owing to the slow rate of decomposition of plant residue because of prolonged periods of ponding of water.

Water retention curves for the soils sampled at the study site are shown in Figure 4.7 and their corresponding air-filled porosities in Figure 4.8. At saturation the water content is usually equal to the total porosity which in turn is related to the bulk density by the relationship  $P_t = 1 - \rho_b/\rho_s$  (where  $P_t$  is the total porosity,  $\rho_b$  is the bulk density and  $\rho_s$  is the particle density). Slight differences can often be ascribed to the presence of unconnected pores within the soil fabric or to a particle density different from the 2.65 g cm<sup>-3</sup> used in the calculation. It is interesting therefore that the saturated water content of the topsoil within the B-Zone was only 0.44 m m<sup>-3</sup>, despite a calculated total porosity of 0.57 m<sup>-3</sup> m<sup>-3</sup>. This difference of 0.13 m<sup>-3</sup> m<sup>-3</sup> is probably linked to increased water repellence in the topsoil, which was especially apparent when attempting to fully saturate the soil during preparation of the cores at the time of measuring the water retention properties. Lignins, tannins and other hydrophobic organic compounds that accumulate on the plantation floor may often form a thin surface seal or coat the internal walls of water conductive pores and so decrease the thorough wetting of the soil. The influence of hydrophobic compounds would also explain why the hydraulic conductivity of this soil is lower than the subsoil which has a smaller total porosity (Table 4.1). Nevertheless the hydraulic conductivity for this soil is generally high due to its good structural stability.

In general there was good correlation between the measured data and the fitted van Genuchten (1980) model results. The shape of the water retention curves are typically "S" shaped with the first inflexion point (closer to saturation) denoting the air entry potential, which for these soils is in the order of -1kPa. This is the potential at which the largest sized pores drain, which from the capillary equation  $P = 2\gamma/r^2$  ( $P$  is the pressure potential,  $\gamma$  is the surface tension of water, and  $r$  is the pore radius) translates into pores with a diameter of 292  $\mu$ m.

As the matric potential decreases, progressively smaller sized pores are drained, the extent of which depends upon the pore size distribution of the soil. Organic matter does influence this relationship by the direct absorption of water but this applies more at high matric potentials. At lower matric potentials, typically nearer the wilting point, water retention is more texturally controlled. It is of interest that the shape of the water retention curves representing the B-Zone soil at a depth of 0.5m and 1.5m are similar implying a similar pore-size distribution (Figure 4.7). This is typical of material having a uniform grade as found at the site. This can also be seen when considering their nearly superimposed air-filled porosity distribution (Figure 4.8).

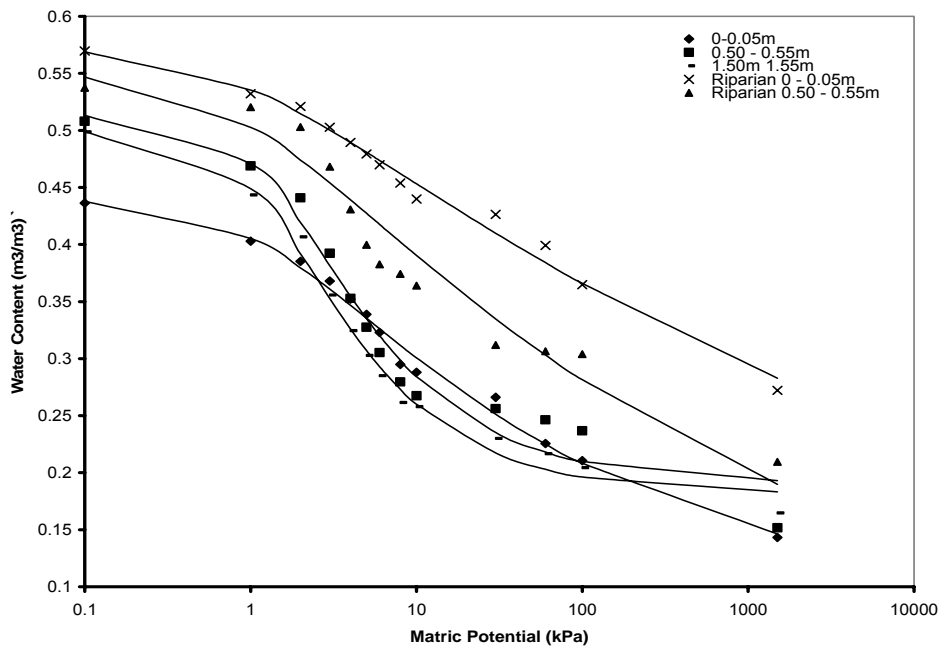


**Figure 4.7** Water retention characteristic for the soils sampled from the B and C Zone at the research site.

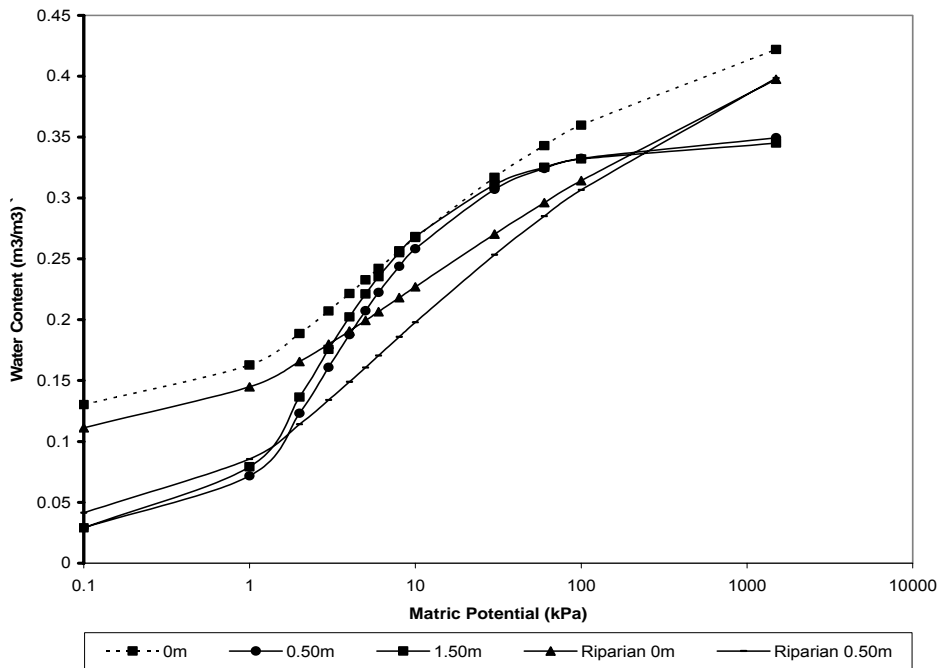


**Figure 4.8** Air-filled porosity for the soils sampled from the B and C Zone at the research site.

It is generally accepted that at field capacity (-10 kPa), where all pores  $> 29.2\mu\text{m}$  are drained, soils with an air filled porosity of around 12 to 15 % would tend to limit root development due to inadequate aeration. From Figure 4.8 it can be seen that none of the soils have an air-filled porosity below this critical limit. On the contrary, in all cases the critical limit is exceeded at a matric potential of only -2 kPa. The air-filled porosity of the B-Zone soil ranged in the order of  $0.24 - 0.27 \text{ m}^3 \text{ m}^{-3}$  at field capacity while the riparian soil was in the order of  $0.20 \text{ m}^3 \text{ m}^{-3}$ . At a matric potential of -100 kPa, when all pores  $> 2.92 \mu\text{m}$  are drained approximately 90% of the total pore space is air-filled, which is indicative of well-structured soil exhibiting good drainage characteristics. Readily available water contents for the B-Zone soil ranged between  $0.3$  and  $0.7 \text{ m}^3 \text{ m}^{-3}$  while the plant available water was in the order of  $0.11$  to  $0.14 \text{ m}^3 \text{ m}^{-3}$ . The riparian soil had a slightly larger plant available water content of  $0.17 \text{ m}^3 \text{ m}^{-3}$  due to the inclusion of medium sized pores in its structure.

### 4.3.2 Monitoring of matric potential

Since the start of this study, soil water potential has been measured every 12 minutes, initially through the tensiometer network and since October 2003 by the watermark system. This has led to the creation of an extensive dataset. In the case of the tensiometers, data processing involves converting the voltage signals from the pressure transducer to water potential by application of a calibration relationship. Although each pressure transducer was calibrated individually there was very little difference in output between these units and so a common calibration curve was adopted. An example of the tensiometer network response to a rainfall event is presented below. The information given is extracted from tensiometer nest 2, located on the south-facing slope just above the riparian zone (Figure 2.3).

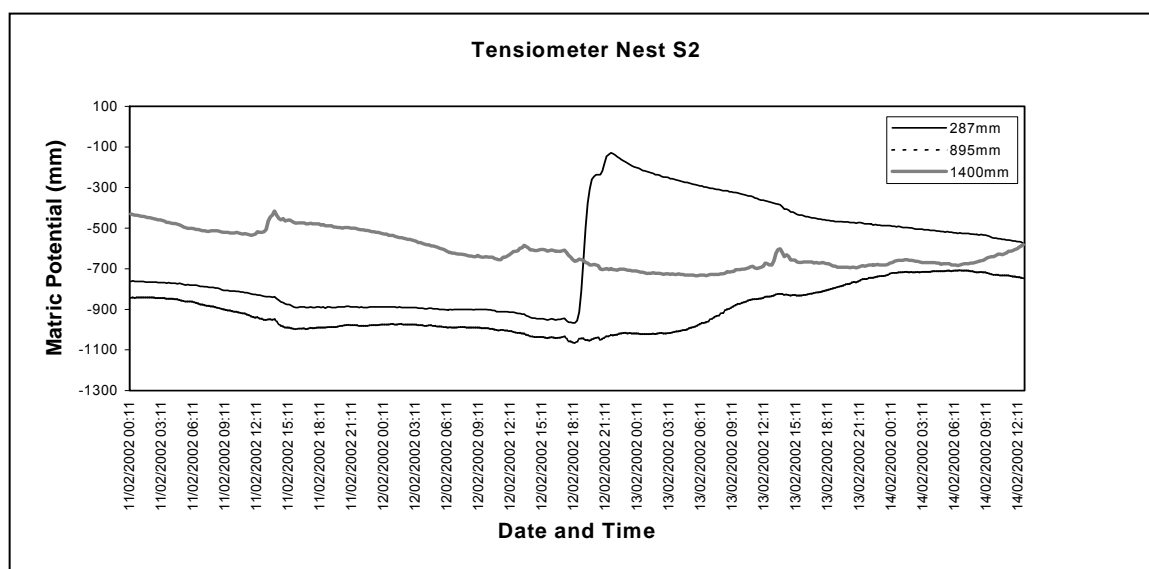


**Figure 4.9** A typical response of tensiometer nest S2 (south facing slope) to a moderate rainfall event

An earlier rainfall event of 19mm on the 8<sup>th</sup> February 2002, which was followed by 0.4mm on the 10<sup>th</sup> February 2002 that caused only the near surface to wet up, accounts for the matric potential in the tensiometer located at the 0.287 m depth being higher than that located at the 0.895m depth. The matric potential in the deeper tensiometer (1.4m) is considerably higher indicating far wetter conditions. Since the start of this event the soil profile has been undergoing a drying sequence denoted by a gradual decrease in matric potential for all soil depths. The rate at which this occurred appears to be very similar for the upper two tensiometers, shown by the nearly parallel response in their respective signals, which implies relatively uniform soil characteristics within this soil depth. The draining sequence for the lower tensiometer (1.4m), however, is interrupted by two brief recharge events (1pm on the 11<sup>th</sup> and 12pm on the 12<sup>th</sup>) as water from the upper soil layers was received at the level of the ceramic.

On the 12<sup>th</sup> of February 2002, 26.6 mm of rain fell within the catchment, 26.4 mm of which was received between 5 pm and 11 pm. This translates roughly into an intensity of 4.4 mm hr<sup>-1</sup>. Within an hour of the onset of rainfall, the near surface tensiometer showed a rapid increase in matric potential from -940 mm at 6 pm to -125 mm at 9 pm, a mere 3 hours later (Figure 4.9). Thereafter, the matric potential decreased, which is to be expected given that the near surface soil wets up first and then transmits water to the deeper layers. The record for the 895mm depth tensiometer shows a more gradual response as the matric potential increased from approximately -1100 mm at the onset of rainfall to a maximum of -745mm just over 24h later (Figure 4.9). The 1.4 m deep tensiometer responded more slowly to

rainfall and only began to show an increase in matric potential from midday on the 13<sup>th</sup> February 2002 onwards. Even so, the matric potential of the soil at this depth reached only – 20 mm at the end of the record, which indicates moderately moist but unsaturated conditions (Figure 4.9).

The data generally show that the south facing slopes remain wetter for longer than north-facing slopes and those areas closer to the riparian zone are wetter than further upslope. To briefly illustrate this finding Figure 4.10 presents information for the same rainfall event extracted from the tensiometer nest located on the upper section of the north-facing slope (N6).

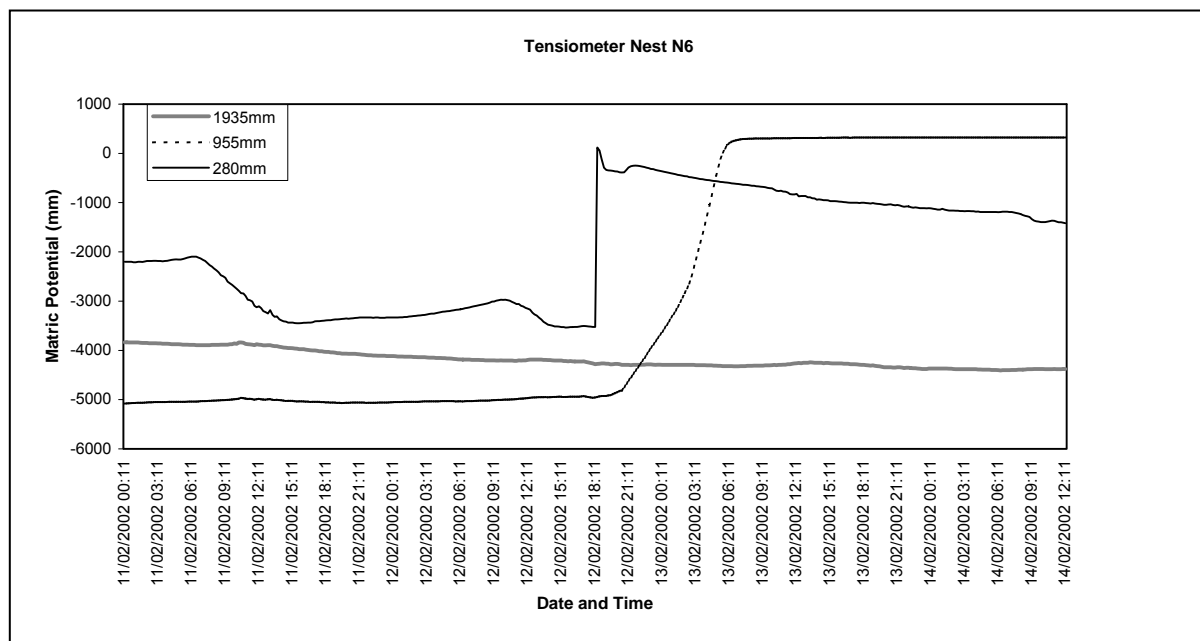


**Figure 4.10.** A typical response of tensiometer nest N6 located on the upper region of the north facing slope to a moderate rainfall event.

An important finding from this data compared with the south facing slope is the much lower values in matric potential that are encountered. For example, at the onset of rainfall (5pm) the 280mm deep tensiometer at nest S2 showed a value of –940 mm matric potential, which contrasts strongly against the –3450 mm recorded by the tensiometer located at the same soil depth further upslope (N6). Nevertheless, the overall reaction of the tensiometer network to the rain event is very similar, although there appeared to be an absent response from the deep tensiometer (1.935 m). The positive value of 289 mm matric potential shown by the 0.955 m deep tensiometer indicates saturated conditions. However, tensiometers located at equivalent depths in nearby nests all indicated unsaturated conditions, which suggests that a localised obstruction within the soil may account for this temporary perched water table.

In November 2004 the watermark system of soil water measurement was extended to the B-Zone mainly due to malfunction of the tensiometers following the deterioration or damage of the ceramic cups. To ensure functionality of the tensiometers regular replenishment of the water within the instrument is necessary in order to maintain good hydraulic contact with the surrounding soil and to eliminate any air-bubbles that may develop in the water columns. However, it was found that the tolerable limit of the instrument (-80 to -90 kPa) was frequently exceeded during the dry periods causing a break in the water column. The effects of servicing the instruments during winter, when the soils are at their driest, lasted for only a few days as water was rapidly evacuated from the tensiometer through the ceramic cup. Given that the watermark sensors have been shown to yield reliable estimates of water

potential at lower matric potentials this system was adopted. Figure 4.11 shows the water potential record for the three watermark sensor banks located within the north facing slope.

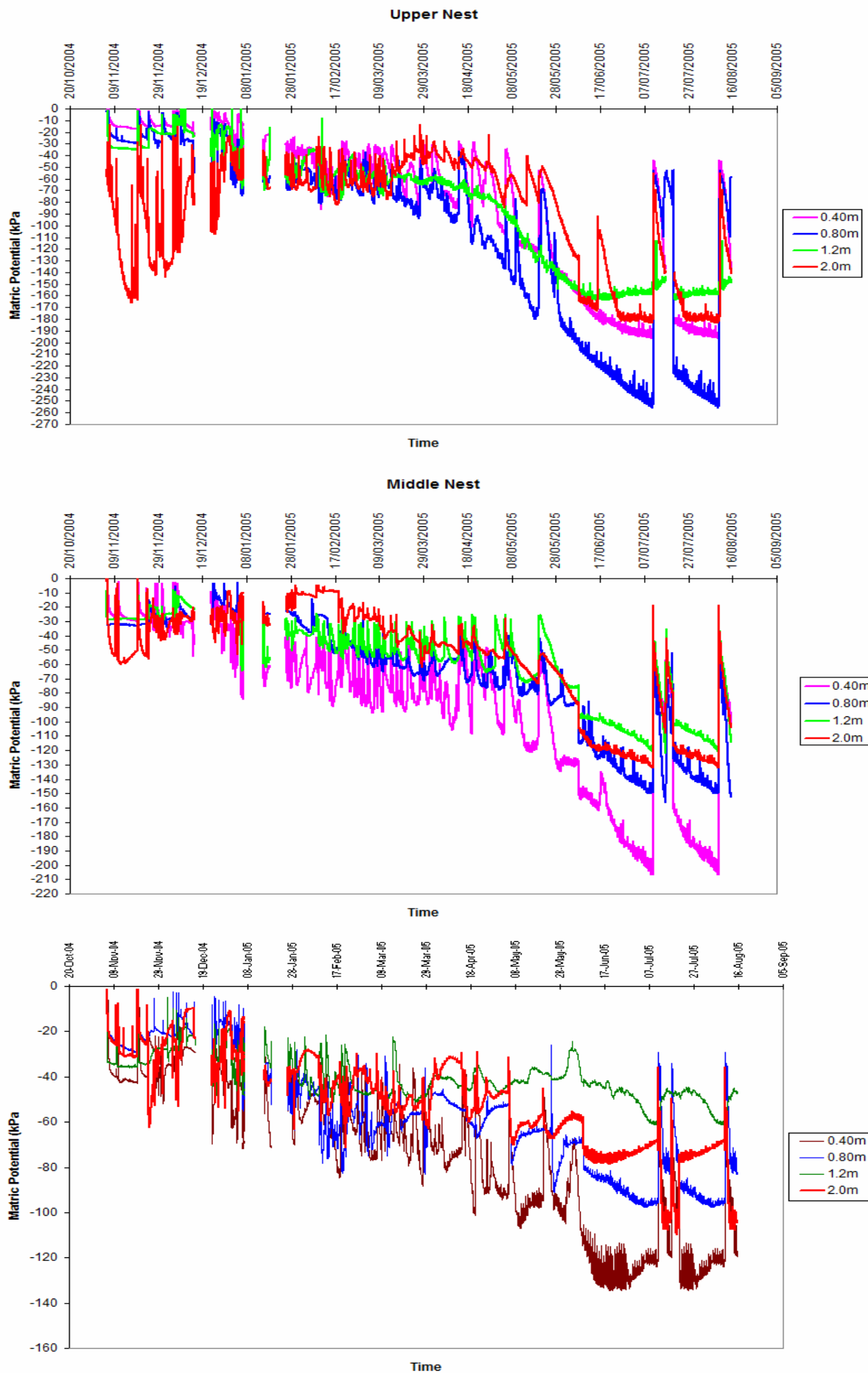


**Figure 4.11** The trend in matric potential for the B-Zone soil of the north-facing slope.

The matric potential of the soil in the B-Zone is strongly seasonal. During summer the upper 1.2m of soil rarely went below -40 kpa indicating fairly wet conditions, mainly in response to the abundant rainfall that was received in the region. Individual rainfall events are often marked by a rapid increase in matric potential followed by a slower rate of drying. Much of the drying phase can be attributed to evaporative demands and drainage to the deeper layers of the soil considering that all of the trees from this portion of the catchment were removed before October 2004. From mid-April onwards, which marks the onset of winter a rapid decrease in matric potential occurs in the absence of any further significant rainfall input and by the end of July the soil in general is at its driest. A further interesting observation from 4.11 is that during summer when rainfall is high the 2.0m soil depth was consistently found to be drier than higher up the soil profile, but a reversal in this trend occurs from the onset of winter where the deeper parts of the soil appear to be wetter. This suggests that during summer which is often associated with short-duration high intensity rainfall episodes much of this water does not infiltrate completely to the deeper layers but rather moves laterally in the near-surface horizon to augment streamflow. Interflow during summer therefore appears to be a significant flow pathway in this catchment. Goller *et al.* (2005) conducted an isotope study tracing water paths through small catchments under a tropical montane rainforest in south Ecuador and found that during normal wet conditions water flows predominantly in a vertical direction through the soil profile to the stream network but during rainstorm events there is a short-term rapid lateral movement of water in the upper layers of the soil. This process could also be aided by the presence of macro-pores and channels in the topsoil formed by the mechanical action of the roots of trees as well as a higher incorporation of organic matter and presumably more intense faunal activity. These conditions would tend to allow water to infiltrate the soil through preferential flowpaths rather than wholly through the soil matrix.

The influence of hillslope topographic position is better evaluated by considering the water potential of the 2.0m deep sensors from the upper, middle and lower nests (Figure 4.12).

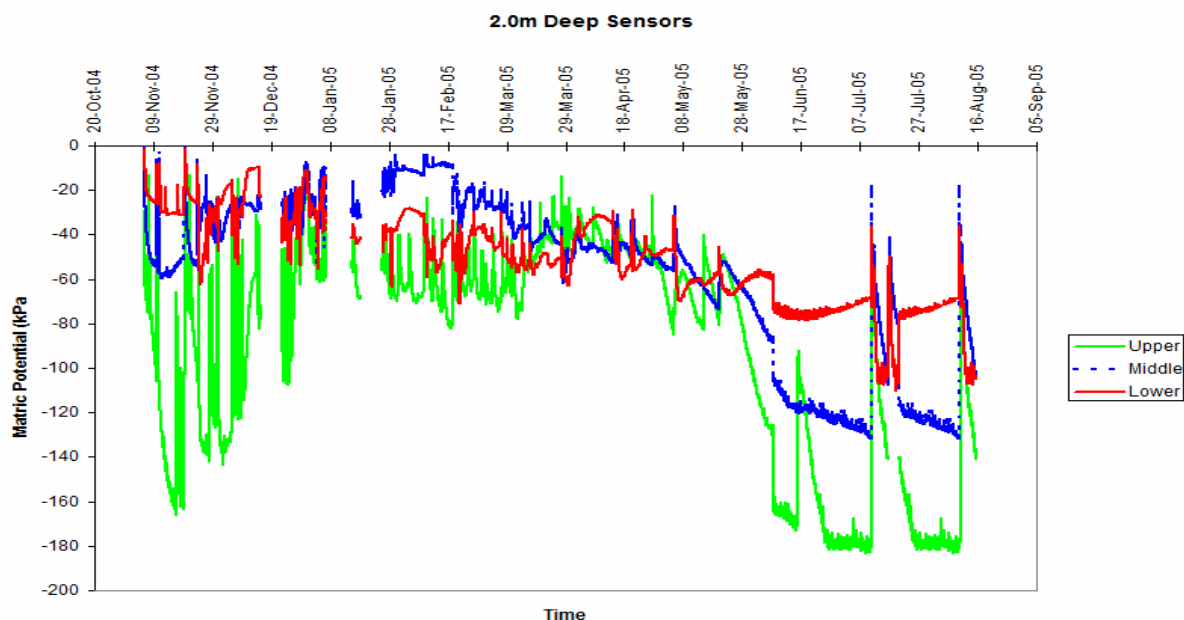


**Figure 4.12** The matric potential of the 2.0m deep soil within the B-Zone of the north-facing slope.

It can be clearly seen that soil located higher upslope within the B-Horizon has a consistently lower matric potential than further downslope and that the nearer one gets to the riparian zone the wetter is the soil at depth. The middle and lower nests show minimum values in matric

potential of -50 kPa compared with -160 kPa for the upper nest although this increased progressively during the course of the summer. An additional reason for the lower nest being wetter may be related to the presence of an upwards hydraulic gradient as water is drawn from the zone of saturation locate deeper within the soil.

Compared to the north facing slope, a similar seasonal trend in matric potential for the south facing slope of the B-Zone is also clearly evident from Figure 4.13.

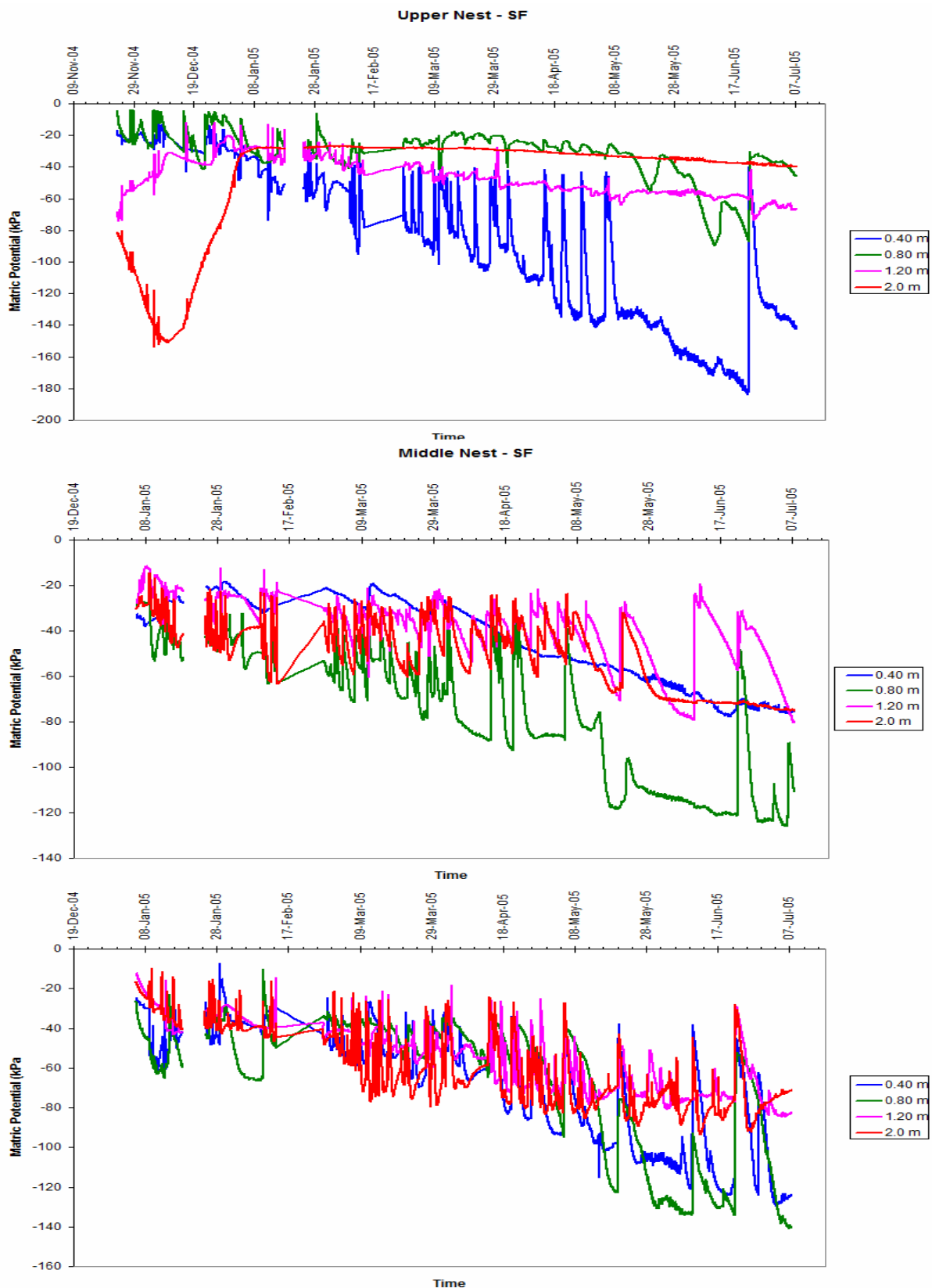


**Figure 4.13** The trend in matric potential for the B-Zone soil of the south-facing slope.

An important observation, however, when comparing the north and south-facing slopes is that the latter on average shows lower matric potential values indicating wetter conditions. This finding is related mainly to aspect as the south facing slope receives on average less radiation than the north facing slope. As was found for the north-facing slope the deeper parts of the soil are drier, albeit to a lesser extent compared with the north-facing slope, than the near surface horizons, but from the onset of winter onwards this trend reverses.

### The A-Zone

The tensiometer record for September 2002 extracted from nest 4, located mid-slope within the A-Zone is shown in Figure 4.14.

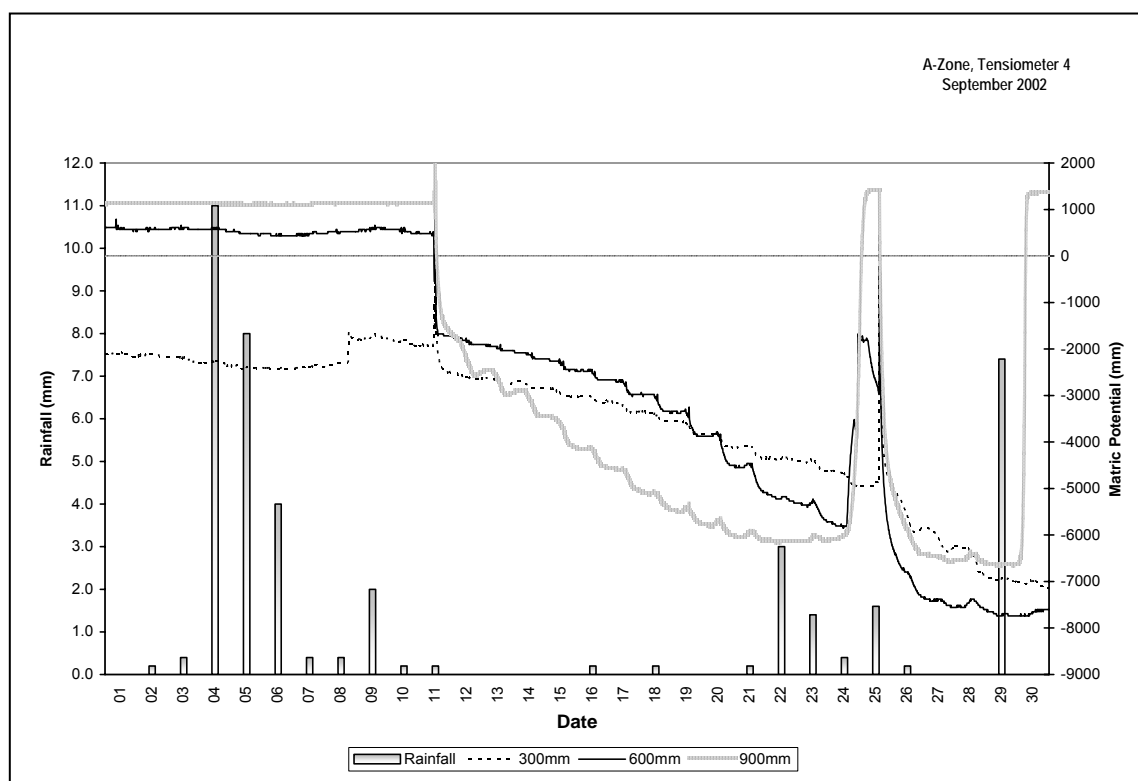


Figure 4.14. Trends in soil matric potential at a mid-slope site within the A-Zone at Two Streams catchment A.

Although 45 mm of rain was received in the area during the last week of August 2002 this was not enough to maintain hydraulic contact between the ceramic tensiometer cup and the surrounding soil. Under these conditions the pressure transducer is sensitive to only the water retained within the column. This is usually expressed by a nearly constant positive matric potential as is shown in Figure 4.11 for the period 1<sup>st</sup> to the 11<sup>th</sup> September 2002. However, the deep tensiometer which continued to function shows a matric potential of -3000 mm, indicating moderately wet but unsaturated conditions.

Replenishment of the tensiometers, an example of which took place on the 11<sup>th</sup> September, are indicated by an almost instantaneous increase in matric potential as the pressure transducer responds to the fully charged water column within the instrument. Since the 11<sup>th</sup> September there has been a slow evacuation of water from the instrument as equilibrium with the surrounding soil progressed. This was interrupted on the 24<sup>th</sup> by a second replenishment event when all of the instruments were once more serviced. Despite the 3mm of rain that was received between the 22<sup>nd</sup> and the 24<sup>th</sup> this was largely undetected by the tensiometer network. These set of events are fairly typical of much of the record that has been collected for the A-Zone with the use of tensiometers, although in general the data does suggest a much

drier soil water regime. Whereas the downslope portion of the hillslope has been shown to stay wetter for longer this does not appear to be the case in the A-Zone.

In October 2003 for reasons cited earlier, the tensiometer network was replaced by the watermark system of soil water monitoring. Since installation of the watermark system a good record of soil water potential for the soils in the A-Zone have been obtained. The data from two of these nests have been extracted for comment, namely nest 3 located midway upslope (Figure 4.15) and nest 1 located at the toe of the slope (Figure 4.16). In addition the response of the sensors from nest 1 to a high intensity rainfall event that occurred on the 12<sup>th</sup> to the 14<sup>th</sup> February 2004 is given in Figure 4.15

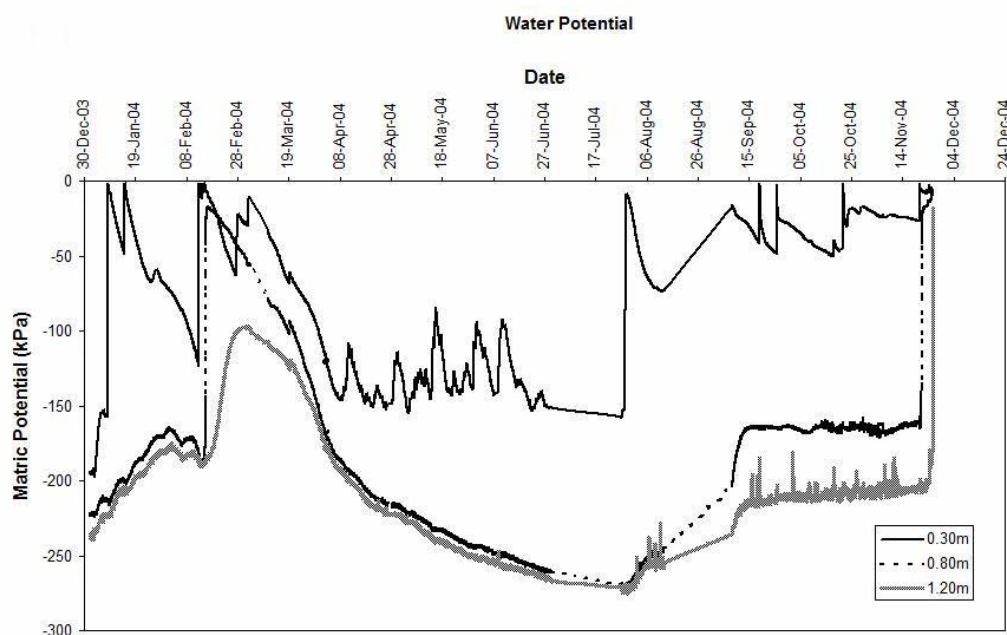


**Figure 4.15:** The matric potential record for nest 3 located in a mid-slope position within the A-Zone

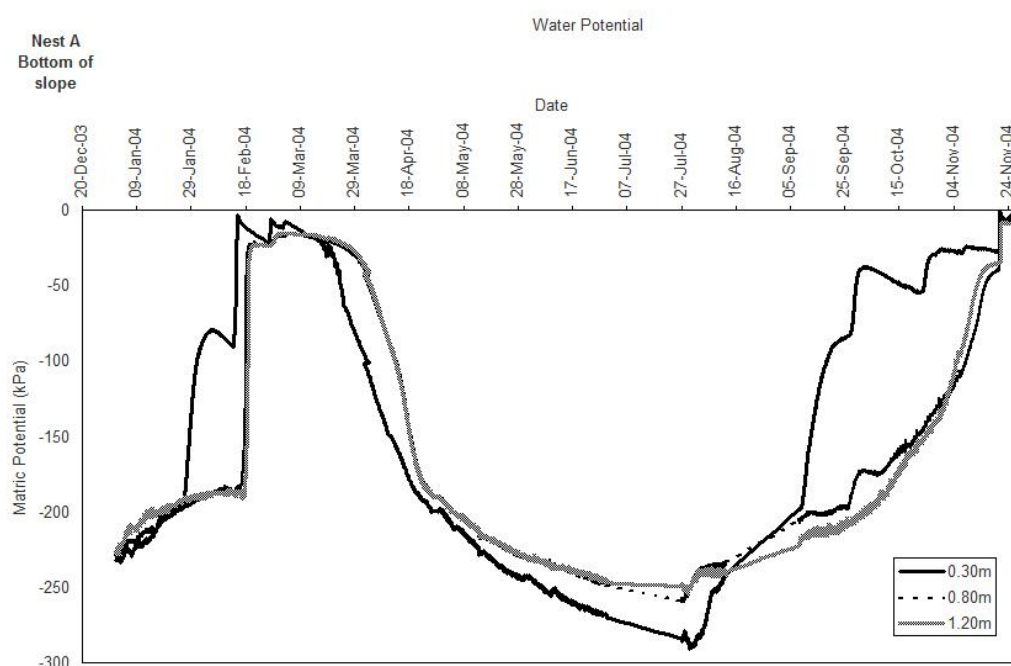


**Figure 4.16:** The matric potential record for nest 1 located at the toe of the slope within the A-Zone

The overall trend in soil matric potential of the A-Zone, as was found elsewhere in the catchment, is strongly seasonal due primarily to the influence of rainfall. As would be expected matric potential values were much higher in summer but decreased significantly during the dry winter months. The matric potential of the topsoil rarely dropped below -100 kPa yet remained in an unsaturated state throughout the summer although values fluctuated strongly because of high evaporative demands and the drainage of water to deeper layers. The presence of several large channels and pores formed by the roots of the trees could have also assisted in the rapid movement of water out of the topsoil. The deeper soil layers, however, which in general were less sensitive to minor rainfall events compared with the topsoil, also showed a steady increase in matric potential as summer progressed but remained fairly dry throughout this period. It was only the large rainfall events that had any meaningful influence on the matric potential of the soil at this depth. Two large rainfall events namely 42.4mm on the 08/01/2004 followed by 45.4mm on the 14/01/2004 accounted for a steady increase in matric potential at a depth of 0.8 and 1.2m.

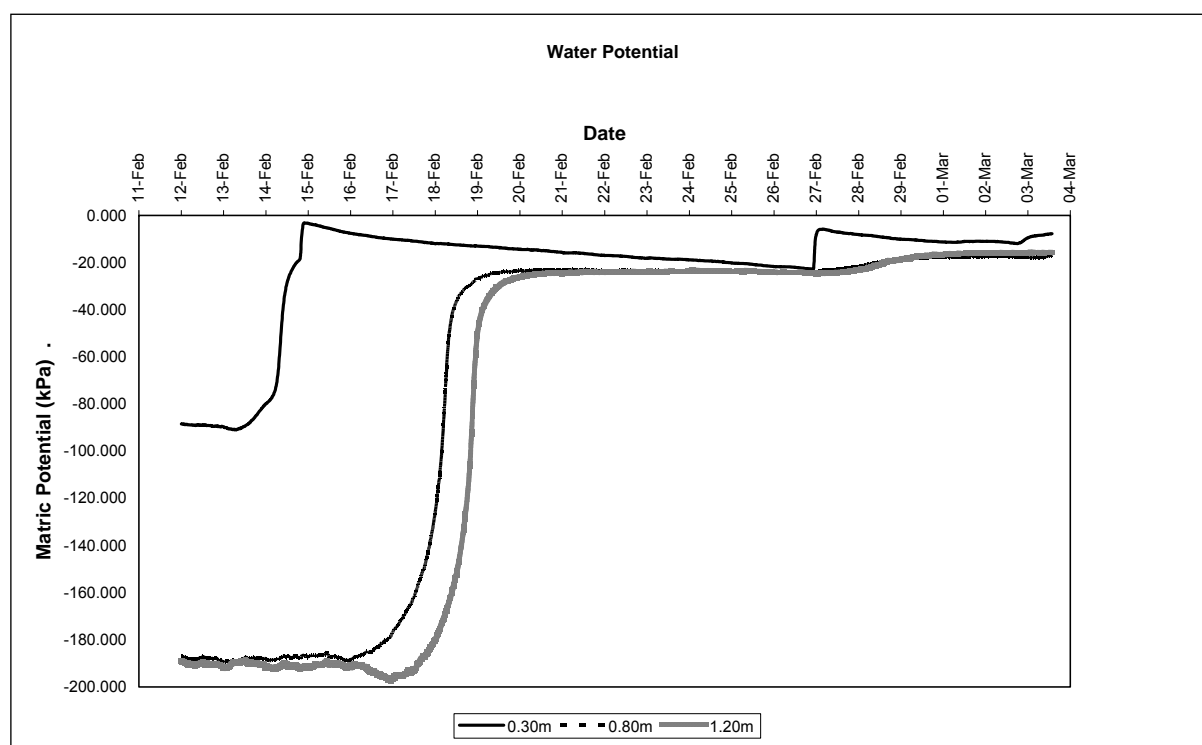


**Figure 4.17:** The response in matric potential at nest 1 to a high magnitude rainfall event.

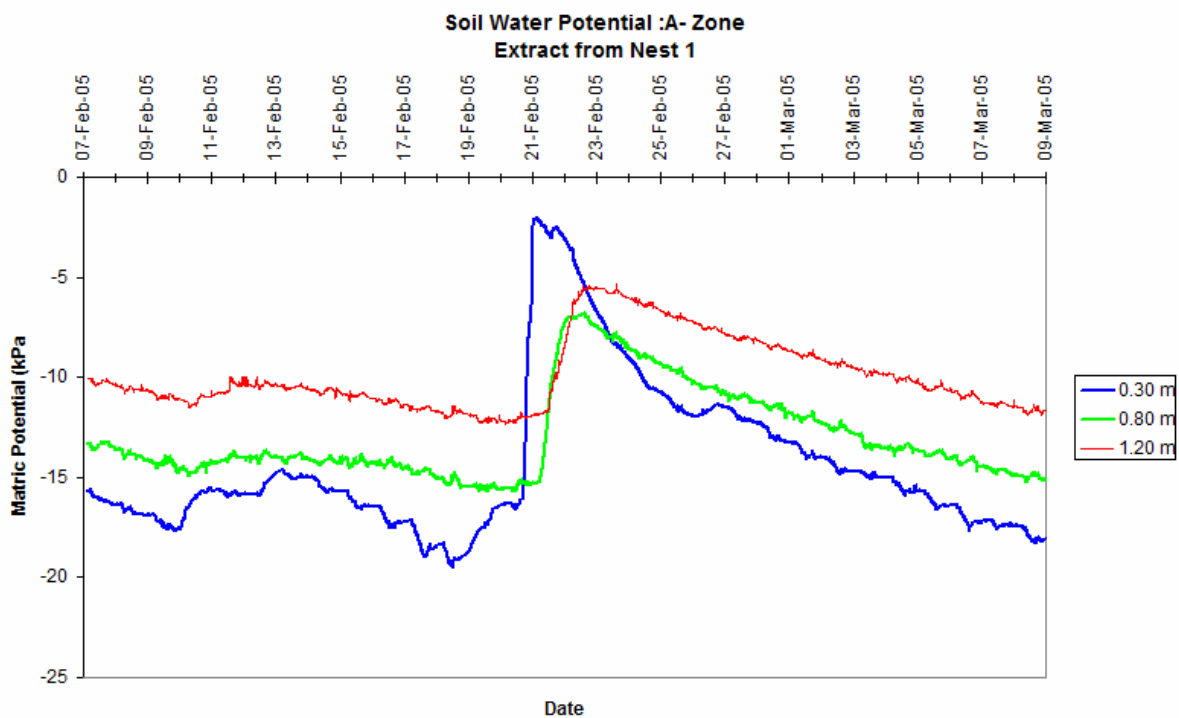
Three days of intense rain totalling 112mm which fell between the 12 and the 14<sup>th</sup> February increased the matric potential of the topsoil at nest 1 from -90 kPa on the 12<sup>th</sup> February to a maximum of -8 kPa on the 15<sup>th</sup> (Figure 4.17). The arrival of the wetting front from this event was detected by the 0.8m deep sensor two days after cessation of rainfall (16<sup>th</sup> February). It took a further three days for the complete passing of this front in which time the matric potential increased from -180 kPa (16<sup>th</sup> February) to a maximum of -27 kPa on the 19<sup>th</sup> February. Similarly the matric potential for the 1.2m deep soil changed from -190 kPa on the 18<sup>th</sup> February as the wetting front reached this depth to a maximum of -35 kPa on the 20<sup>th</sup> February. The 1.2m deep sensor at nest 3, located in a mid-slope position, shows a more gradual response in the rate at which the matric potential increased reaching a maximum of just under 100 kPa towards the end of February. This is probably due to the lag that occurs as water is received from higher up the soil profile.

Since the onset of winter the matric potential of the soil across all depths decreased steadily. Brief episodes of rain maintained the topsoil at nest 4 within the -150 to -100 kPa range but this effect was absent at nest 1 at the toe of the slope. Since the end of the rainfall period

(19<sup>th</sup> March) the topsoil at nest 1 has been drying out at a higher rate than for the deeper soils and by mid June this had reached a minimum of -300 kPa. Much of this effect can be attributed to the loss of water from the soil by evaporative demand. A brief episode of rain at the end of August caused an increase in the matric potential of the topsoil although this had less of an effect for the deeper layers. In general the matric potential record for the soil at the A-Zone suggests much drier soil conditions than further down the slope.

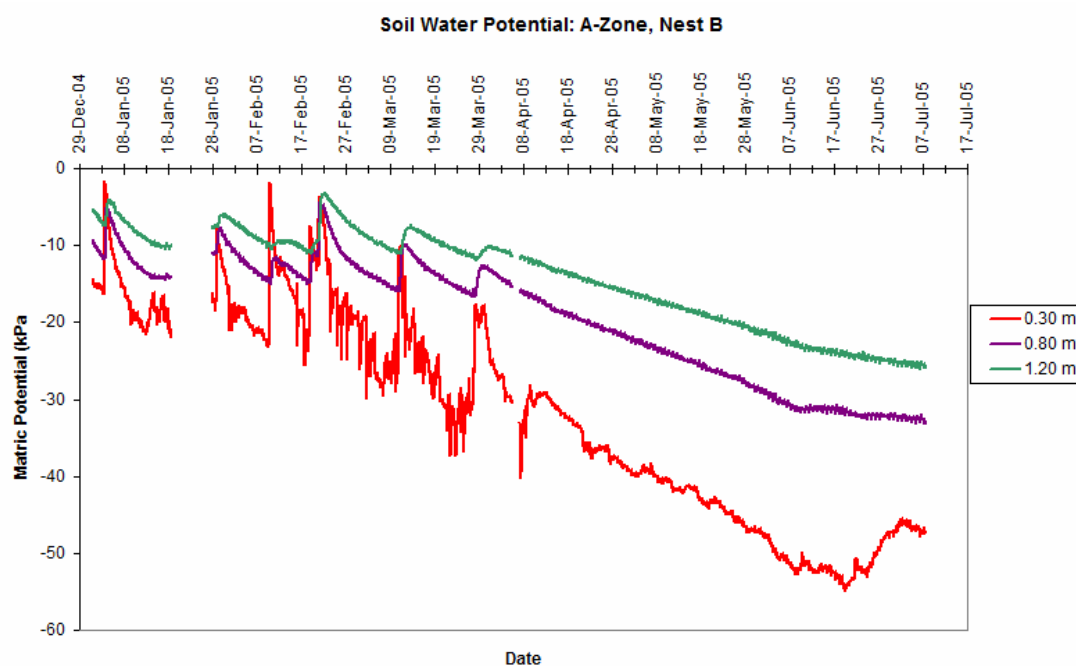
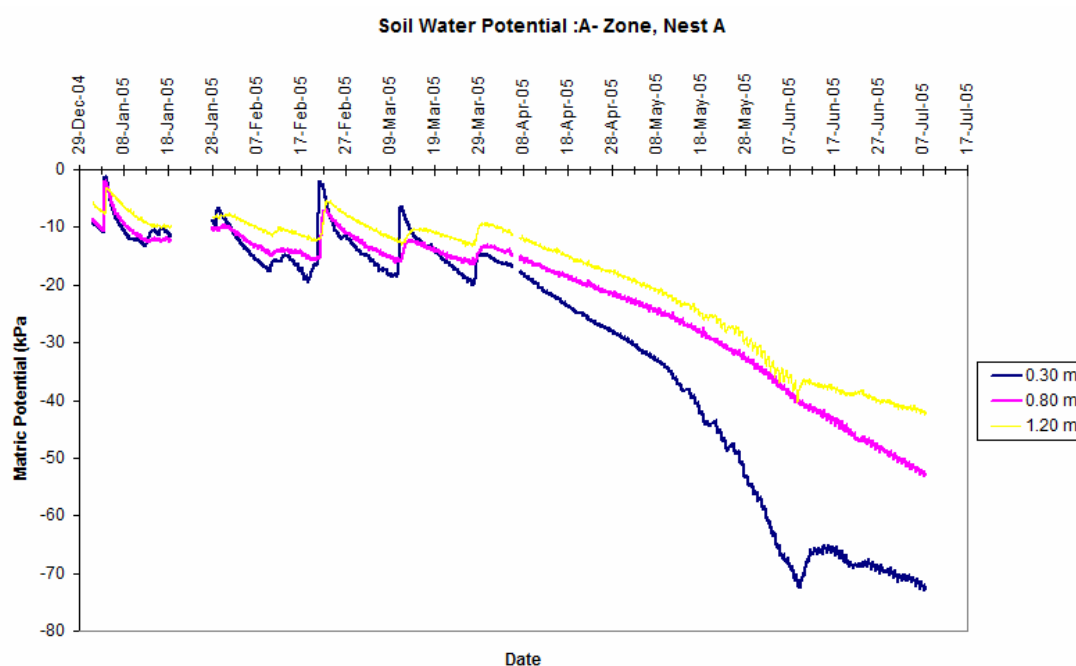
Figures A to E present the matric potential record for nests A to E within the A-Zone for the period 29/12/2004 to 17/07/2005. Nest A is located at the foot of the slope and Nest E approximately 60m upslope. All nests are sited along a common longitudinal transect. During summer when rainfall is abundant the matric potential of the soil remains high, rarely dropping to below -20kPa. At this matric potential all soil pores greater than 58.4  $\mu$ m are water-filled. Numerous recharge events caused a rapid increase in soil water status which is progressively reduced by the evaporation of water and percolation to the deeper soil layers.

An example of such an event is given in Figure 4.18, which shows the soil's reaction to a 48.4 mm event that occurred on the 20<sup>th</sup> February 2005. In the week immediately preceding this event the matric potential of the 0.30m, 0.80m and 1.20m soil depths averaged approximately -18, -14 and -10 kPa respectively. The onset of rainfall during the early hours of the 20<sup>th</sup> February increased the matric potential of the topsoil from an initial value of -17kPa to a maximum of 3kPa by noon of the 21<sup>st</sup>. The passage of the wetting front was detected by the 0.80m deep sensor in the early hours of the morning of the 22<sup>nd</sup> and by the 1.2m deep sensor by noon of the same day. The recession or drying part of the curve is interesting as it shows that even though the topsoil wets rapidly, it also dries rapidly. Whereas the 0.80m and 1.20m deep sensors show a similar rate of decrease in matric potential, the 0.30m sensor shows a marginally higher rate owing essentially to evaporative demands and drainage.



**Figure 4.18:** The reaction of the soil at Nest A within the A-Zone to a 48.4 mm rainfall event

By the end of March which coincides with the onset of winter, a rapid drying out of the soil occurs. The rate at which this takes place is clearly fastest for the topsoil for reasons cited earlier and by early June the soil has reached its probable lower limit in matric potential. Interestingly the topsoil remained the driest part of the soil profile throughout the winter and although minor rainfall events did cause a slight increase in matric potential, this was insufficient to cause any meaningful change in the seasonal average. The deeper parts of the soil remained much wetter throughout the winter with an average matric potential of -40 kPa. The rate at which this soil depth dried out was also slower. The influence of topographic position on soil water status can be seen by comparing the topsoil matric potential across the different sensor nests. In nest A, B and C the matric potential for the topsoil does not drop lower than -80 kPa whereas the topsoil at nests D and E, further up the slope, dries to approximately -110 and -230 kPa respectively. Since the A-Zone of the catchment is rarely, if ever, in contact with the water table this finding shows that at higher topographic locations within the catchment, lateral movement is an important regulator of soil water status.



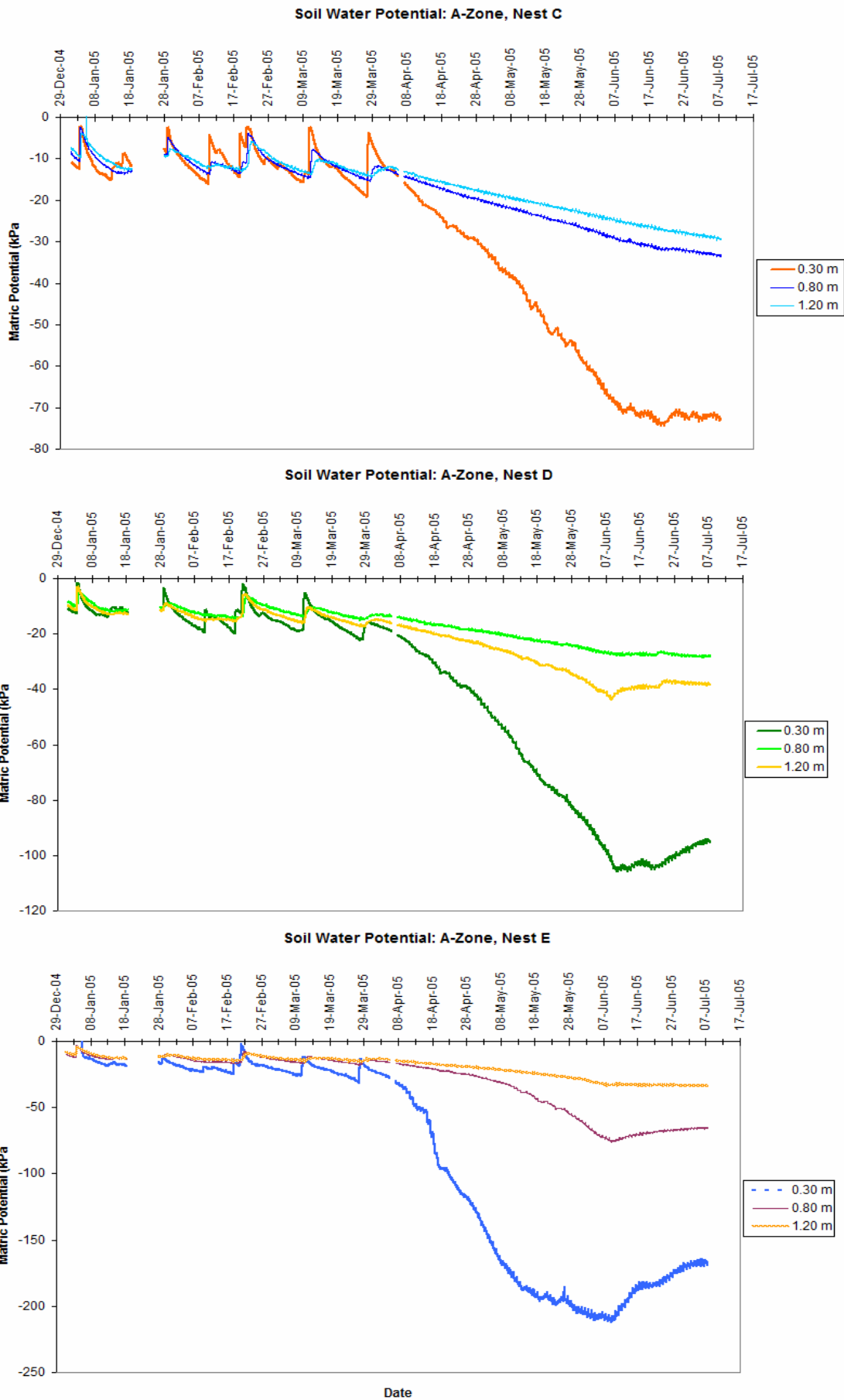


**Figure 4.19.** The trend in matric potential for the soil in the A-Zone. Sensor nest A is located furthest downslope whereas sensor nest E is located furthest upslope. All nests are sited along a common transect.

The removal of the trees by the end of July 2004 appears also to have had a positive influence on the soil water status of the A-Zone. If one considers the record in soil water potential for the period prior to removal of the trees against that obtained after the catchment was clear-felled (Figures 4.15 and 4.18) then it can be seen after clearfelling, the soil matric potential on average was higher. For example during the winter of 2004 the soil water potential at a depth of 0.80 and 1.20 m reached a minimum of -260 kPa (April to July) whereas in the following winter (2005) the minimum matric potential was substantially higher at around -30 kPa. Although differences in rainfall between the 2004 and 2005 hydrological year could have had a bearing on this finding it does suggest that forestry does have a strong influence on soil water status.

### Riparian Zone

An early activity in this study was the removal of the trees from the riparian zone. Since then, this part of the catchment has been maintained fallow although re-colonisation of the native vegetation occurred to some extent. The effect of this approach on soil water potential of the riparian zone is shown in Figure 4.20 for the latter part of the 2004 summer and the winter of 2005.

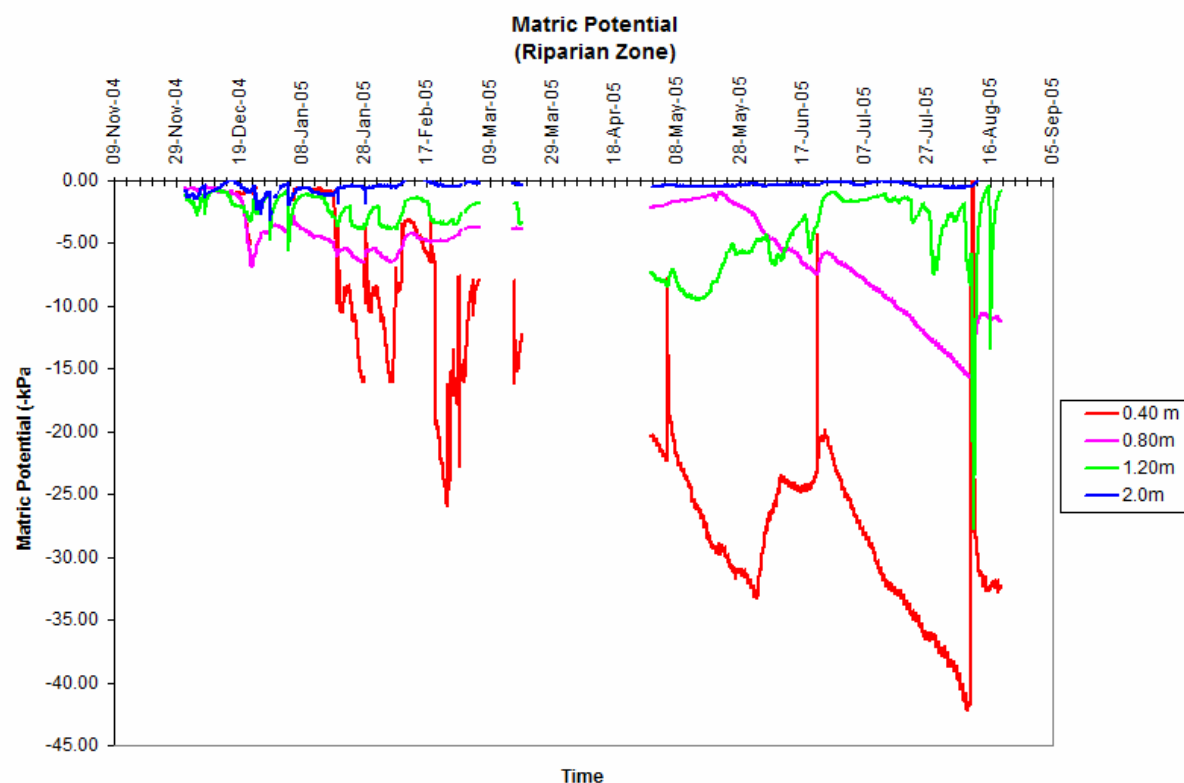


**Figure 4.20.** The matric potential of the riparian zone soil for the period November 2004 to September 2005.

Compared to elsewhere in the catchment (B and A-Zone) the soil within the riparian zone is much wetter. On average the 1.20m deep soil remained close whereas the 2.0m deep soil was permanently saturated even during winter. Seasonal fluctuations in water potential are more accentuated for the upper part of the soil (0 -0.80 m) as it is this part of the soil environment that would be subject to the greatest evaporative demands. Even so the water potential of the topsoil only reached a minimum of -40 kPa during mid-winter. The rate at which the water potential of the topsoil decreased following the onset of winter was also much lower than the B and A-zone portions of the catchment. These findings therefore corroborate quantitatively the generally accepted view that riparian zones are an integral component of the catchment responsible for the regulation of streamflow and that these systems need to be protected to ensure adequate water supply. Apart from the tensiometer network, five neutron probe

access tubes were also installed within the site to an approximate depth of 5.5m to measure the water content of the soil at deeper levels. An example dataset of the information obtained is given in Figure 4.21. These data show that the soil water content is strongly linked to rainfall. Several high intensity rainfall events during the month of December caused an increase in soil water content for most soil depths. Whereas the shallower soil depths show this trend with far greater clarity, the deeper soil depths have more of a gradual response due mainly to the time it takes for the water at the soil surface to infiltrate to these deeper layers. It is interesting; however, that the 0.30m soil depth in general is drier than the lower depths which suggest that soil water evaporation is an important process accounting for the rapid drying out of the soil.

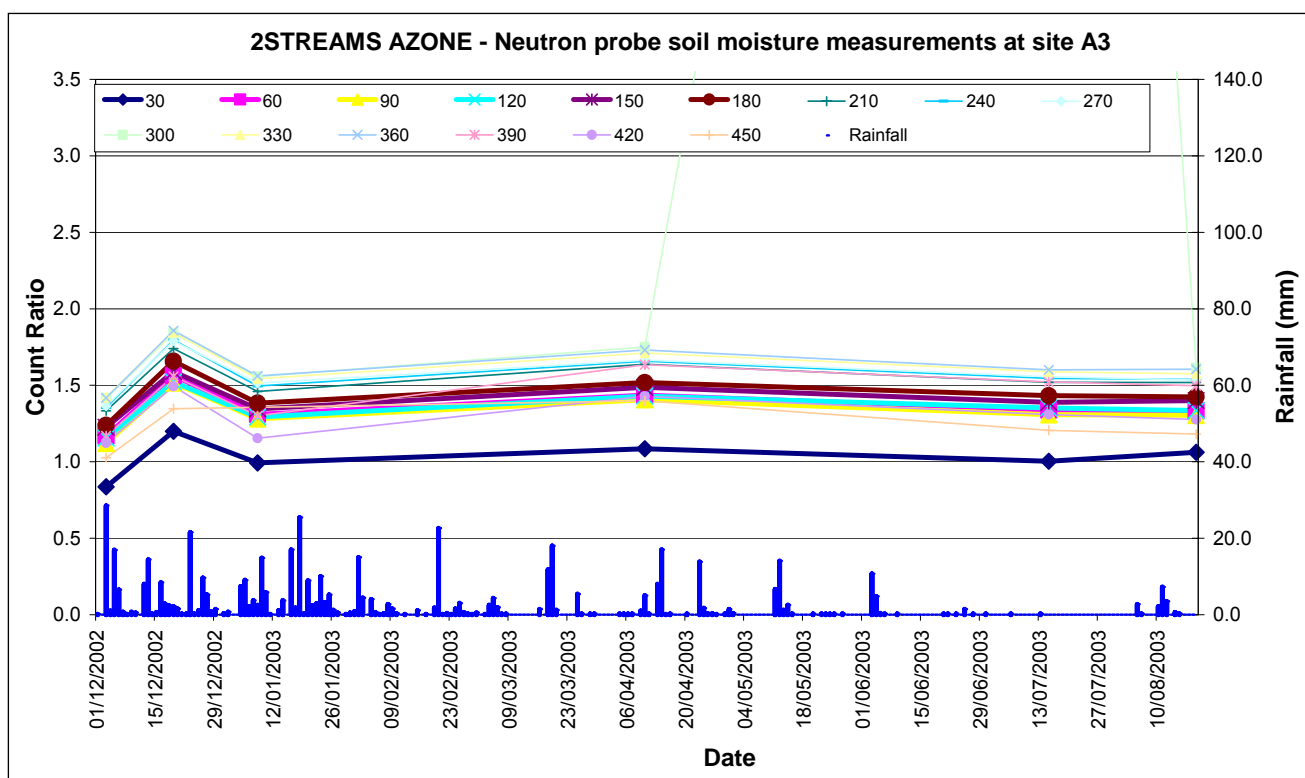


**Figure 4.21.** Trends in soil water content at the A zone site (December 2002 to August 2003).

#### 4.4 Ground Water Monitoring

Fluctuations in water table depth with time for the various boreholes, as well as flow rates from the deep aquifer are illustrated in Figure 4.22. Ground water levels in the upslope sites have shown little seasonal variation over the three year monitoring period. However, the water table in the riparian zone has risen from 350 mm in July 2000 to 245 mm below the surface at the end of the 2003 dry season, a significant increase of 105 mm, despite the low rainfall in the latter part of the 2003 monitoring period. Interestingly the flow from the deep aquifer has showed a steady decline over the same period. This decline in flow rate may be from a larger regional aquifer, making interpretation of the results difficult. This decline in flow rate has flattened out during the 2004 study period.

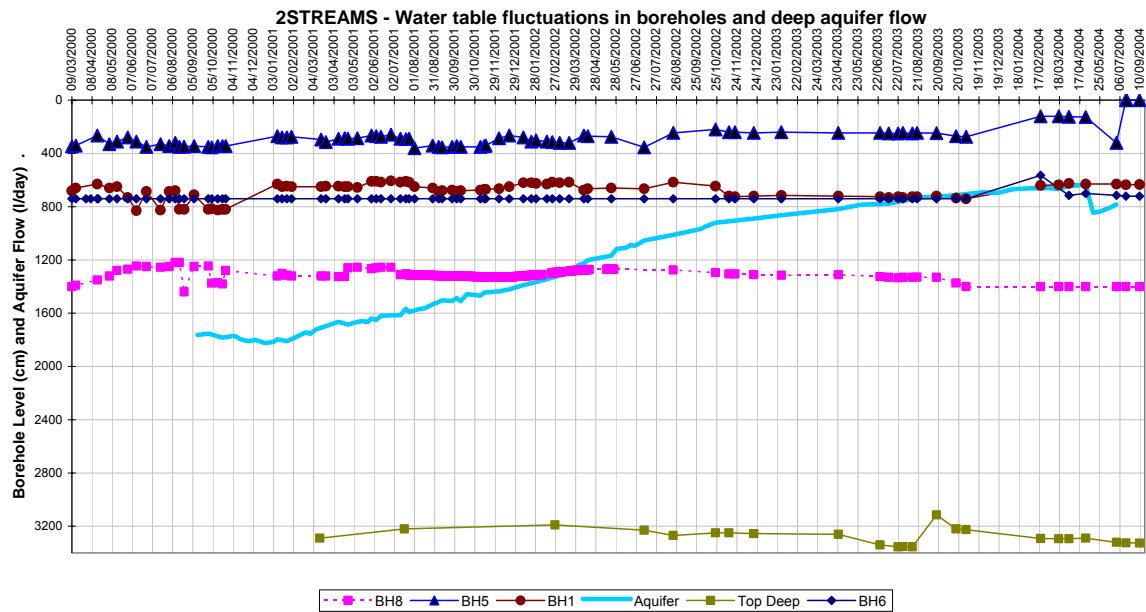


**Figure 4.22.** Ground water levels at various hillslope positions in the two stream A-catchment.

#### 4.5 Surface runoff

During the reporting period the surface and subsurface runoff from the A-zone has been monitored using a runoff plot. Total surface and subsurface runoff during the reporting period was only 2034 and 376 l respectively. Clearly there is very little runoff from this portion of the catchment. The removal of the trees will provide an interesting contrast. An example of a rainfall-runoff event is shown in Figure 4.23. During this event 13.4 mm of rainfall was recorded, producing only 75 l of surface runoff. Six similar events have now been monitored, all showing similar trends, with the timing of the runoff and rainfall being closely linked.

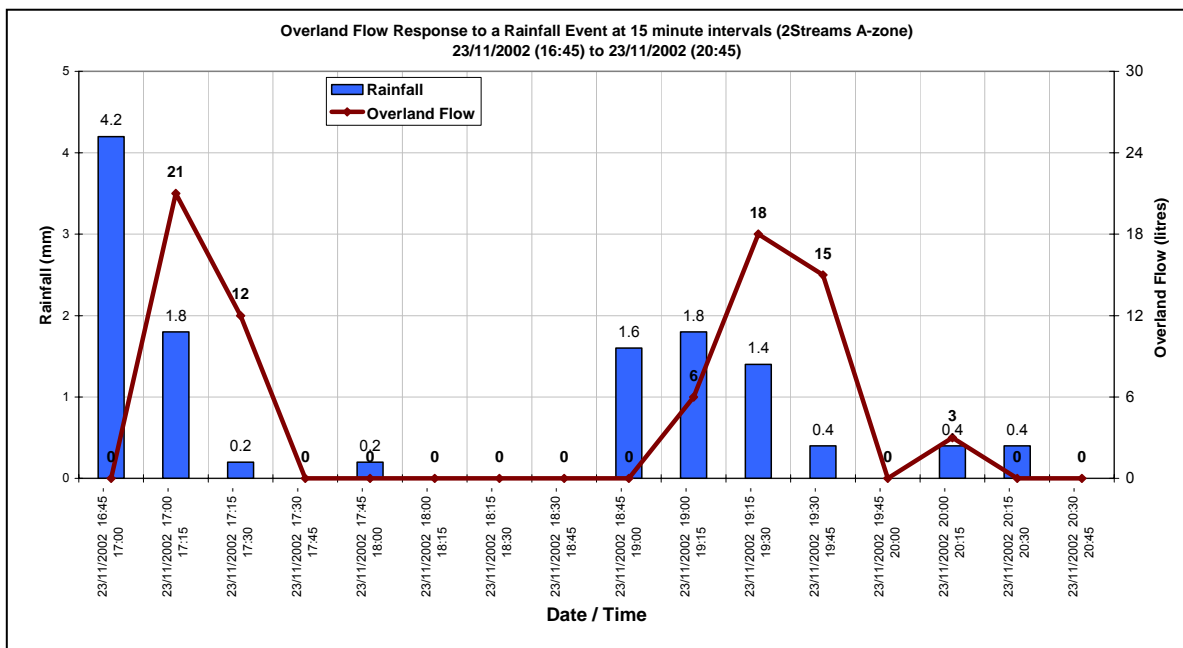


**Figure 4.23.** A surface runoff and rainfall event in the A-Zone during November 2002.

#### 4.6 Sap flow studies in the wattle trees

Water balance studies in other South African research catchments have shown that the loss of water from vegetation (evapotranspiration) is commonly in the range of 45 to 80% of precipitation. Consequently, it is very important to quantify the rate of ET in order to correctly assess the storage and movement of soil and groundwater towards the stream. Sap flow measurements have been concentrated in two mid-slope areas of the catchment representing north and south-facing slopes, respectively.

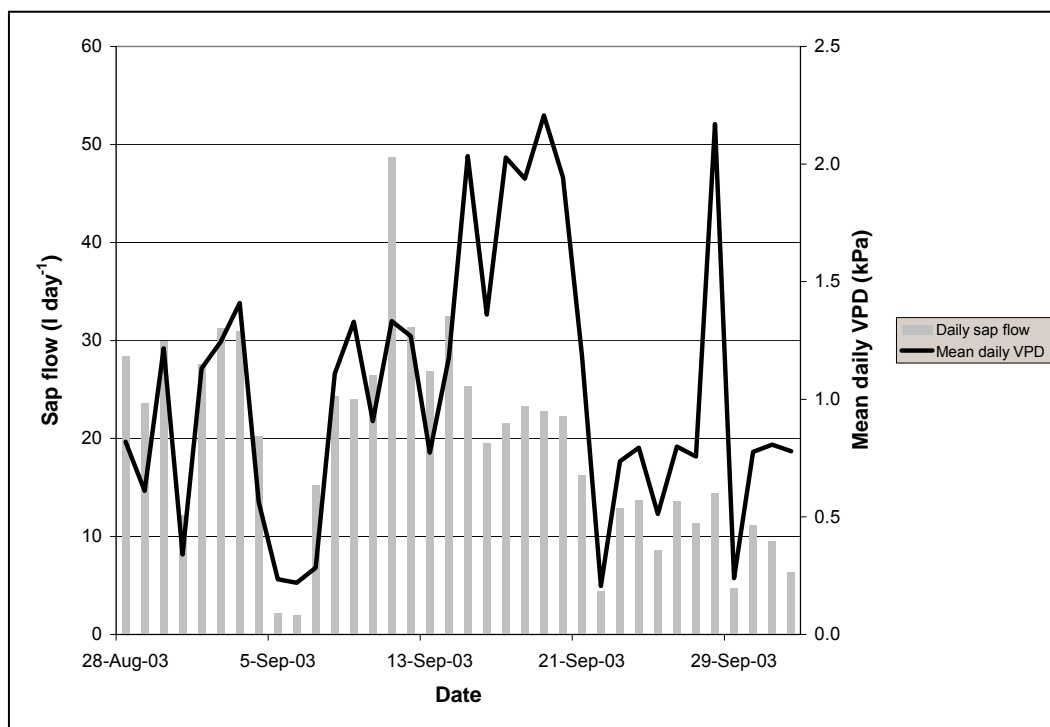
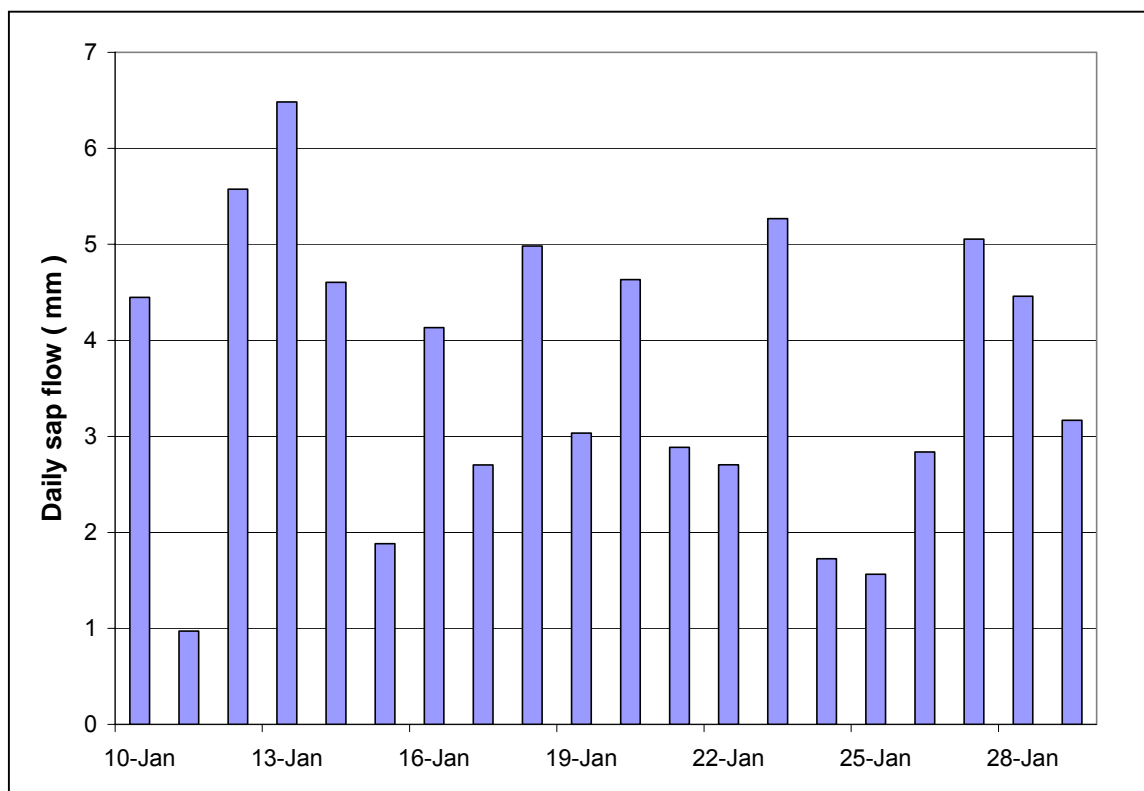


**Figure 4.24** Sap flow measured in the A-Zone (August to September 2003).

An early finding in this study was that wattle trees (in contrast to eucalypts and pines) reacted strongly to the presence of heat pulse probes inserted in the sapwood. Severe resin exudation around the probes, as well as growth distortions in the sapwood, required that the sample trees be changed every two to three months. Each new cycle of measurement starts with a survey of tree diameters to choose four new sample trees that represent four size classes of tree. After probes have been installed and data logger programmed for hourly readings during daylight hours, the equipment is left to run automatically, and checked at fortnightly intervals. Once growth distortions are visible in the trunk, the probes are removed and implanted into new sample trees. After felling the old sample trees, a section of trunk is cut and brought back to the laboratory to determine the sapwood properties that are required to convert heat pulse times to whole-tree sap flow. All required information for a complete analysis of past sample tree HPV data are available and ready for analysis. A Hobo sensor has provided a continuous record of temperature and air humidity on the south-facing slope.

Past experience has shown that wattle sap flow is highly correlated to the local air humidity, and this relationship is very useful in detecting periods of bad data and patching gaps with modelled sap flows. Figure 4.24 shows the relation between mean daily humidity (vapour pressure deficit, VPD) and total daily sap flow recorded in three sample trees representing the range of tree size on the south-facing slope of the catchment. The measurements span the period from 9 – 30 January 2002, which is close to mid-summer and therefore represents the highest rates of sap flow expected in the course of the year. Daily sap flow is closely related to mean daytime VPD, indicating that the trees regulate their leaf transpiration rates to avoid

excessive water loss under dry atmospheric conditions. Sap flow is proportional to tree diameter, since larger trees have greater leaf area and better exposure to sun and wind. Very similar patterns have been reported in two other tree sap flow studies in South Africa (Dye, 1996; Dye *et al.*, 2000).



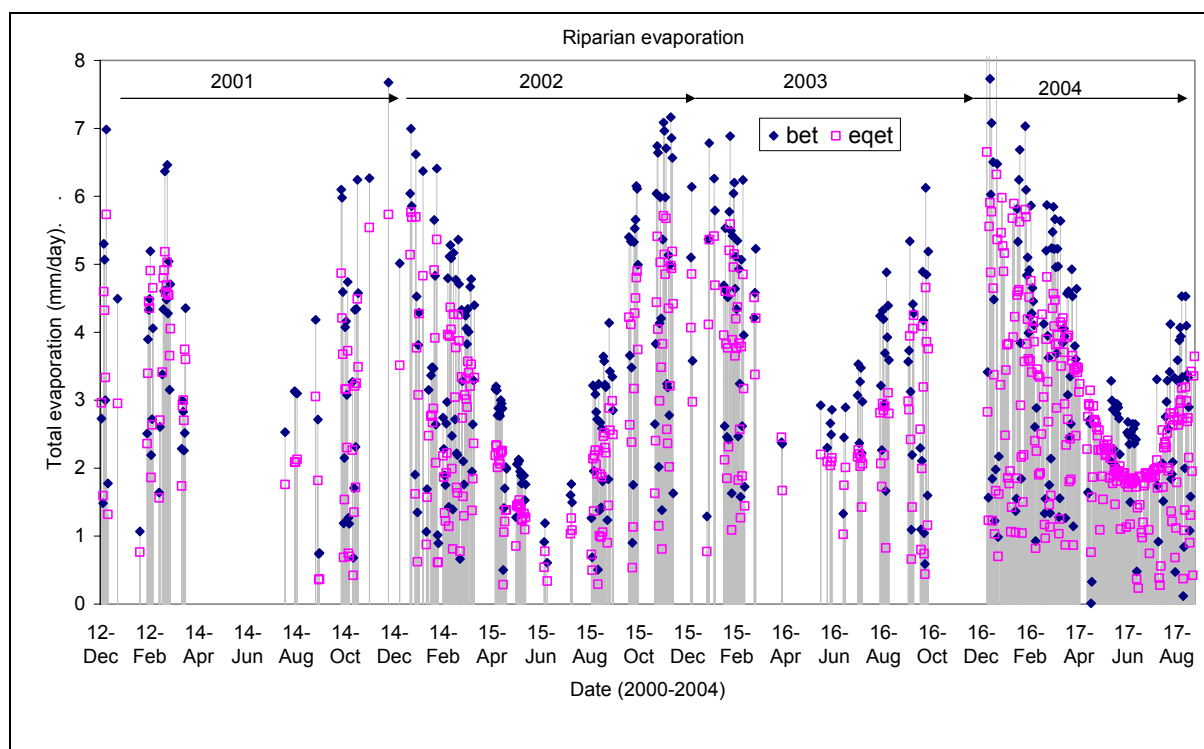
**Figure 4.25.** Daily ET (mm) estimated for the period 10-29 January 2001 for the south-facing *Acacia mearnsii* in the research catchment.

Figure 4.25 shows the estimated plot ET over the same period. A mean daily sap flow for the whole compartment of trees was calculated for each day by averaging the sample tree daily flows, after adjusting these according to the proportions of each size class in the surrounding compartment. This mean daily sap flow ( $l\ tree^{-1}$ ) was then multiplied by the number of trees per hectare (1116) and divided by the total land area ( $10000\ m^2$ ) to yield daily ET in units of mm equivalent depth of water. This varies from 1 to 6.5  $mm\ day^{-1}$  in response to changes in daily air humidity. The maximum compares favourably to numerous other reported rates of maximum daily ET, which commonly vary from 5-7  $mm\ day^{-1}$  (Dye and Bosch, 1999).

Measurements of sap flow were discontinued in the original north and south facing slopes, due to scheduled clearfelling. In June 2002, a fresh sample of four trees was selected within the “A zone” site on the north-facing slope of the catchment to provide information on tree transpiration rates. These sample trees were chosen to represent four size classes of trees spanning the entire range of tree size recorded in the general vicinity. Heat pulse probes were implanted in each sample tree, and hourly heat pulse velocities recorded thereafter until 12 November 2002. Previous experience has shown that longer periods of sap flow measurement are not possible, since wounding responses in the tree severely disrupt the flow of water in the sapwood adjacent to the probes. The sample trees were felled to measure the necessary sapwood characteristics in the area where the probes were implanted.

#### 4.7 Grassland evaporation in the cleared riparian strip.

Evaporation of the recolonised natural grassland in the cleared riparian strip has been monitored using the Bowen ratio energy balance technique. Data have been analysed for the period December 2000 to September 2004 (Figure 4.19). This represents a good data set, which will be used to parameterise the Penman-Monteith equation for the riparian zone. The grassland evaporation ranged between 3 and 6.5 mm day<sup>-1</sup> during this period showing the large contribution of the grassland to water use within the catchment during the summer period (Figure 4.26). Clear trends of low evaporation in the dry winter period followed by peak rates in mid summer are shown by these data. It is during the winter period, when the grass has senesced, that the wattle trees will be expected to use more water. These data do however illustrate the very high water use (summer maxima >6 mm day<sup>-1</sup>) of the predominantly dense *Setaria megaphylla* vegetation in the riparian strip.



**Figure 4.26.** Daily evaporation in the grassland site from December 2000 – September 2004.

#### 4.8 Geophysical survey using ground penetrating radar.

The first samples (13/07/00) showed curves indicating a descending rock interface dipping as the stream was approached which then disappeared (Figure 4.27). The fact that they disappeared does not make sense for this hill slope position. It may possibly be explained by the presence of the ground water table. The range chosen for these transects may also have been too high. These data did not provide a confident assessment of the depth to the bedrock.

A second attempt (03/08/00) to gain data using a different range, showed similar results, with curves going down and disappearing as the stream was approached. The range of 100 ns was more precise but did not allow a very deep scan (about 4m).

Interpreting a GPR samples is notoriously difficult and requires training and practice. Traces from Two streams were taken to experts in Pretoria for interpretation, but this did not help to clarify the interpretation. Because of the large uncertainties around these results, the final interpretation will be made when more detailed geological information is available. The

project team will also investigate the use of the Soil Resistivity technique as an alternative, due to the uncertainty generated by the GPR data.

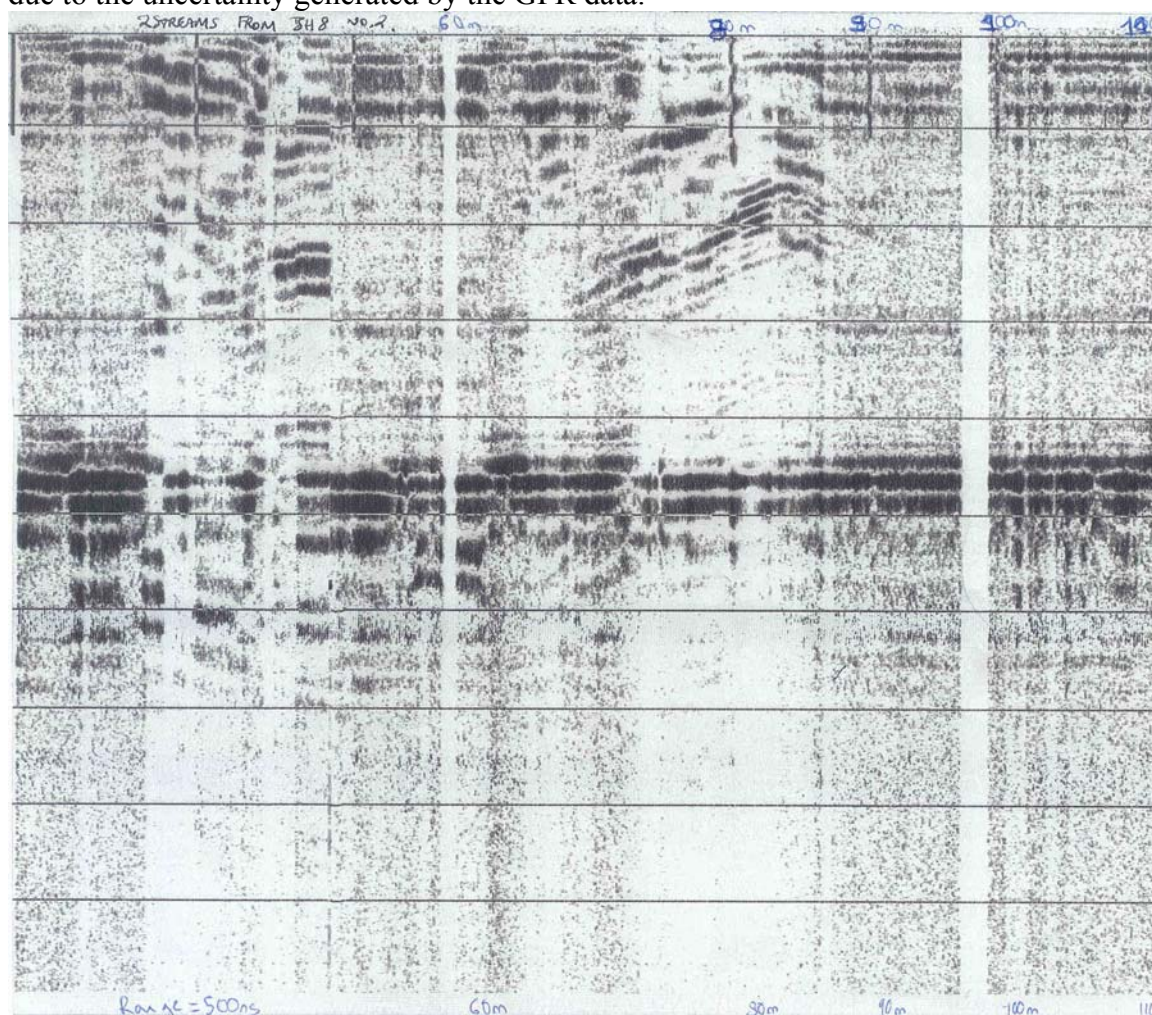


**Figure 4.27** An example of a GPR depth profile taken along a transect in the 2 streams catchment A.

## 4.9 Catchment scale modelling

### 4.9.1 Introduction

The forest hydrology group of the CSIR has identified the need for suitable hydrological models to assist in predicting the impact of land and water management alternatives. Because of the complex mosaic of different landuses in most catchments, the need for a spatially explicit model was also identified. Thus the chosen model had to be integrated with recent advances in geographic information systems (GIS) and other spatial analysis software. Many hydrological models are widely available, but few have been seamlessly integrated into the GIS environment. One such model is the Soil Water Assessment Tool (SWAT), developed at the Blackland Research Centre in Texas for the USDA Agricultural Research Service.

The SWAT model is a daily time step model and some of its key strengths lie in the ability to predict the relative impacts of changes in management practices, climate and vegetation on water quantity and quality. The aim of this aspect of the project was to conduct a verification of the SWAT model using the Two Streams Catchment data and to carry out long term simulations on the impact on streamflow of *acacia mearnsii* on the hydrology of the study catchment.

#### 4.9.2.1 Background to the SWAT model

Full details of the model are given in Arnold et al., 1999 and Neitsch et al., 2001, and therefore only a brief outline of the concepts and general structure of the SWAT model are included here. The model is a continuous daily time step model developed to simulate the long-term impacts of land and water management (e.g. reservoir sedimentation over several years) or agricultural practices (e.g. crop rotation, planting and harvesting dates and irrigation). It is physically based and uses readily available inputs and is computationally efficient to operate on large catchments within a reasonable time. SWAT allows a number of different physical processes to be simulated in a catchment, which may be grouped into the following major divisions:

- Hydrology, weather and soil temperature,
- Sedimentation,
- Crop growth,
- Nutrients and pesticides, and
- Agricultural management.

The model may simulate a catchment in lumped or distributed mode, by automatically delineating the catchment either into subcatchments or hundreds of grid cells based on a Digital Elevation Model (DEM). The use of subcatchments in a simulation is particularly beneficial to differentiate the impact of various landuses and soils on the hydrology of a catchment. The development of the model as an extension to Arcview has increased the flexibility of the model, with the special features of Arcview also being available to SWAT model users. Other data requirements include:

- spatial coverage for landcover and soil types,
- daily precipitation, and
- daily maximum and minimum temperature.

SWAT 2000 also has options to use measured solar radiation, wind speed, relative humidity and evaporation data. Daily rainfall and temperature data may be generated if unavailable or missing for the simulation period from statistical data in the weather generator file. There are no limitations to the number of rainfall and temperature gauges that can be used in the simulation (Neitsch et al., 1999). The model includes a number of storage databases, which may be customized for an individual catchment. Included are soils, landcover/plant growth, weather stations, pesticides, tillage, fertilizer and urban datasets. A single growth model in SWAT is used for simulating all crops based on a simplification of the EPIC crop growth model (Williams et al., 1984). Phenological development of the crop is based on daily heat unit accumulation, with the growing season being defined by date or accumulated heat units. The model can simulate up to 10 soil layers if sufficiently detailed information is available. SWAT 2000 is also acknowledged for the ability to model across a range of timescales i.e. hourly, daily, monthly and annual time step (Neitsch et al., 2001).

#### 4.9.2.2 Background to the ACRU model

##### Concepts and Structure of the *ACRU* Agrohydrological Modelling System

The *ACRU* agrohydrological model is a multipurpose, daily time step, physically-based model. It has a multi-layer soil water budgeting routine, with outputs that include streamflow, sediment yield, reservoir yield, irrigation supply and demand, as well as a daily water balance. The *ACRU* model was originally developed in the early 1980s for studies of land use change and water resource assessment, and has subsequently undergone continuous development and enhancement. It is well suited to use in Southern Africa, with links to appropriate land use, soil and climate databases.

*ACRU* can operate in lumped mode for smaller catchments or as a distributed cell-type model for areas with more complex land uses or soils. Individually requested outputs for each subcatchment which may be different to those of other subcatchments or with different levels of information may be generated. The multi-layer soil water budgeting accounted for in the model by partitioning and redistribution of soil water is depicted in Figure 4.28 (Schulze, 1995).

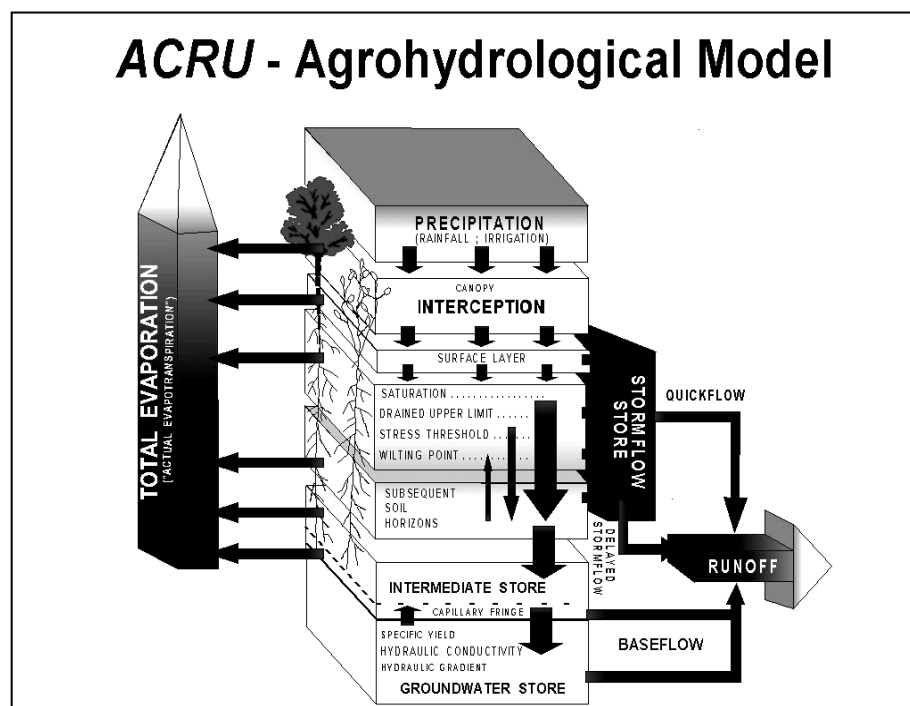


**Figure 4.28** General structure of the *ACRU* agrohydrological modelling system

The model also includes a dynamic input option to facilitate modelling the hydrological response to climate or land use management changes in a time series, be they long term/gradual changes e.g. forest growth, urbanisation, climate trends or abrupt changes e.g. clear felling, fire impacts or construction of a dam. *ACRU* also operates in conjunction with interactive *ACRU* Utilities, is a suite of software tools to aid in the preparation of input and output information e.g. Menubuilder (to compile catchment menus for *ACRU* application), CALC\_PPTCOR (to facilitate selection of appropriate rainfall stations), AUTOSOILS (to extract appropriate relevant soil characteristics) and Outputbuilder (to select the relevant output variables for graphical or statistical analysis as displayed in Figure 4.29 (Schulze, 1995).

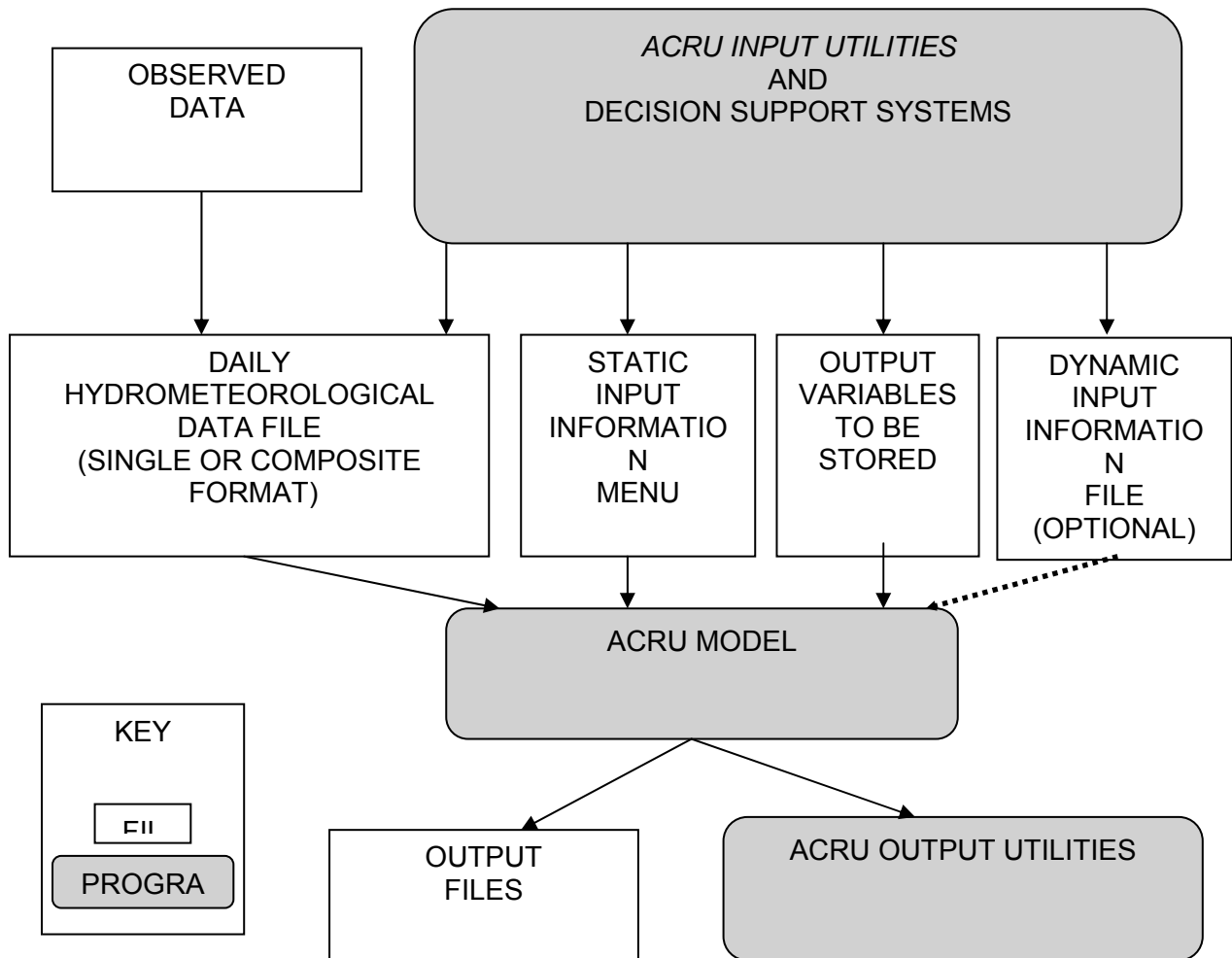


**Figure 4.29** Components and structure of the *ACRU* modelling system. The version of the model used in this study was *ACRU 331*.

### 3.2 Streamflow Simulation by *ACRU*

Streamflow generated by the *ACRU* model comprises of baseflow and stormflow. Stormflow consists of a quickflow response which is released into the stream on the same day as the rainfall event, and delayed stormflow response or post-storm interflow. Baseflow is derived from the groundwater store which is recharged by drainage out of the lower active soil horizon when its water content exceeds the drained upper limit (Schulze, 2000).

The estimation of stormflow depth is based on the equation derived by the Soil Conservation Services (United States Department of Agriculture, 1985) and Schmidt and Schulze (1987) cited by Schulze (1995),

$$Q = \frac{(P_g - I_a)^2}{P_g - I_a + S} \text{ for } P_g > I_a$$

where,

- $Q$  = stormflow depth (mm)
- $P_g$  = gross daily precipitation amount (mm)
- $I_a$  = initial abstractions (mm) before stormflow commences
- $S$  = potential maximum retention (mm).

There are several conceptual differences between the original SCS stormflow equation and

the form in which it is used in the *ACRU* model noted by Schulze (1995):

- Interception is abstracted separately and before the commencement of potential runoff-producing rainfall, and is not part of the initial abstractions as in the SCS model.
- The coefficient of initial abstraction (COIAM) is a parameter in the model, which may be varied monthly, and is dependent on rainfall intensity, vegetation, site and management characteristics. A default value of 0.2 is suggested.
- The potential maximum retention  $S$ , is calculated as a soil water deficit by the multi-layer soil water budgeting routines of *ACRU* as the difference between water retention at porosity and the actual soil water content just prior to the rainfall event assumed to occur at the end of the day.
- A coefficient of quickflow response (QFRESP), has been included in the model to account for any lagged response caused by for example catchment size, soils with high or low interflow potential, steep or urbanized catchments, and different vegetation types. Therefore this parameter acts as a decay function controlling the timing or distribution of stormflow over one or several days but does not control the total amount of stormflow.
- The critical soil depth (SMDDEP), for which the soil moisture deficit is calculated for stormflow generation attempts to account for different dominant streamflow producing mechanisms due to different catchment conditions. Figure 7 suggests values for SMDDEP according to differing climate, vegetation and soil characteristics.

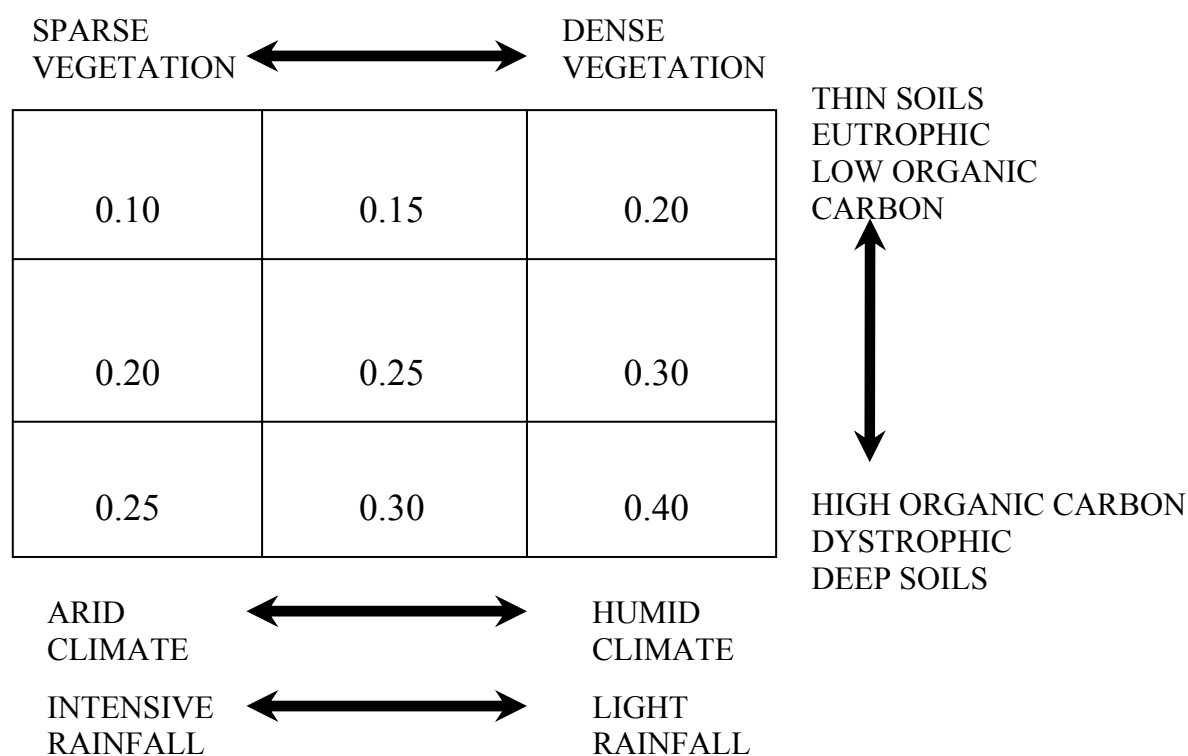


**Figure 4.30** Suggested values for SMDDEP according to climatic, vegetation and soils characteristics (after Schulze, 1995)

With regard to baseflow generation the following response coefficients have been incorporated into the model:

- ABRESP, which determines the rate at which water drains from the A- to B-horizon.
- BFRESP, which similarly controls the rate of drainage from the B-horizon to the groundwater store.

- Lastly, the coefficient of baseflow response (COFRU), which determines the rate at which water in the groundwater store is released as the baseflow per day.

Evaporation takes place from previously intercepted water as well as simultaneously from the various soil horizons. It is either spilt into separate components of soil water evaporation (from the topsoil only) and plant transpiration (from all horizons in the root zone), or combined as total evaporation or actual evapotranspiration. Soil water evaporation for a day can either be occurring at maximum rate, if a minimum threshold of soil water resides in the topsoil horizon, or below the maximum rate once soil water has dried, in which case soil water evaporation declines very rapidly with time. Evaporation demand on the plant is estimated according to atmospheric demand through reference potential evaporation and the plant's growth stage. The roots absorb soil water in proportion to the distributions of root mass density of the respective horizons, except when conditions of low soil water content prevail. In such cases the relatively wetter soil horizons provide higher proportions of soil water to the plant in order to obviate plant stress as long as possible.

#### 4.9.3 Data Sources

Digital Elevation Models (DEMs) of a fine resolution are not freely available in South Africa. Therefore 1:5000 scale contour maps for the study sites were digitized and used to create DEMs in ArcInfo. DEMs having a 10 m resolution were produced. Soils were obtained from the ISCW database and Mondi soils maps. Landuse layers were obtained from the GPS data collected during the mapping exercise.

Long term daily rainfall and temperature data from 1950-2000 were used in the model simulations. The data were obtained from the daily rainfall and temperature databases developed by the University of Natal's School of Bioresources Engineering and Environmental Hydrology.

#### 4.9.4 Model Configuration

Because of the small size of the catchment only one hydrological response unit (HRU) based on the predominant soils and landuse data was delineated by the model. The model was setup to utilize SWAT's landcover classes listed in the landcover database, but modified to represent South African conditions. Sugar cane, wattle, veld and eucalyptus vegetation types were configured for the SWAT growth model.

Potential Evapotranspiration (ET) was estimated using the Penman Monteith formulation (Monteith, 1965). Where the Penman-Monteith method required solar radiation, air temperature, windspeed and relative humidity as inputs, the data were simulated using a weather generator file, created from the Seven Oaks automatic weather station daily data. Measured daily temperature data were used, while monthly averages of solar radiation, windspeed and relative humidity values were retrieved from the weather generator file.

The model was configured to test three different scenarios: 1. Complete afforestation with *Acacia mearnsii* (including trees in the riparian zone) 2. Removal of the *Acacia mearnsii* trees from the riparian zone and 3. Natural veld (Baseline condition).

#### 4.9.5 Results

Annual rainfall for the fifty year period showed a clear cyclical trend in the rainfall pattern with three peaks occurring in about 1961, 1976 and 1997 (Figure 4.31). The high rainfall of 1987 (1438 mm) are also prominent in the data. Streamflow followed the cyclical rainfall pattern, with values generally less than 20 mm in dry years (e.g. 1970-72) and between a 100-250 mm in wet years. Predicted streamflow in 1999 was only 4 mm (Figure 4.31), and coincides with observations from this project of no visible streamflow at this time (see Figure 5 in January 2000).

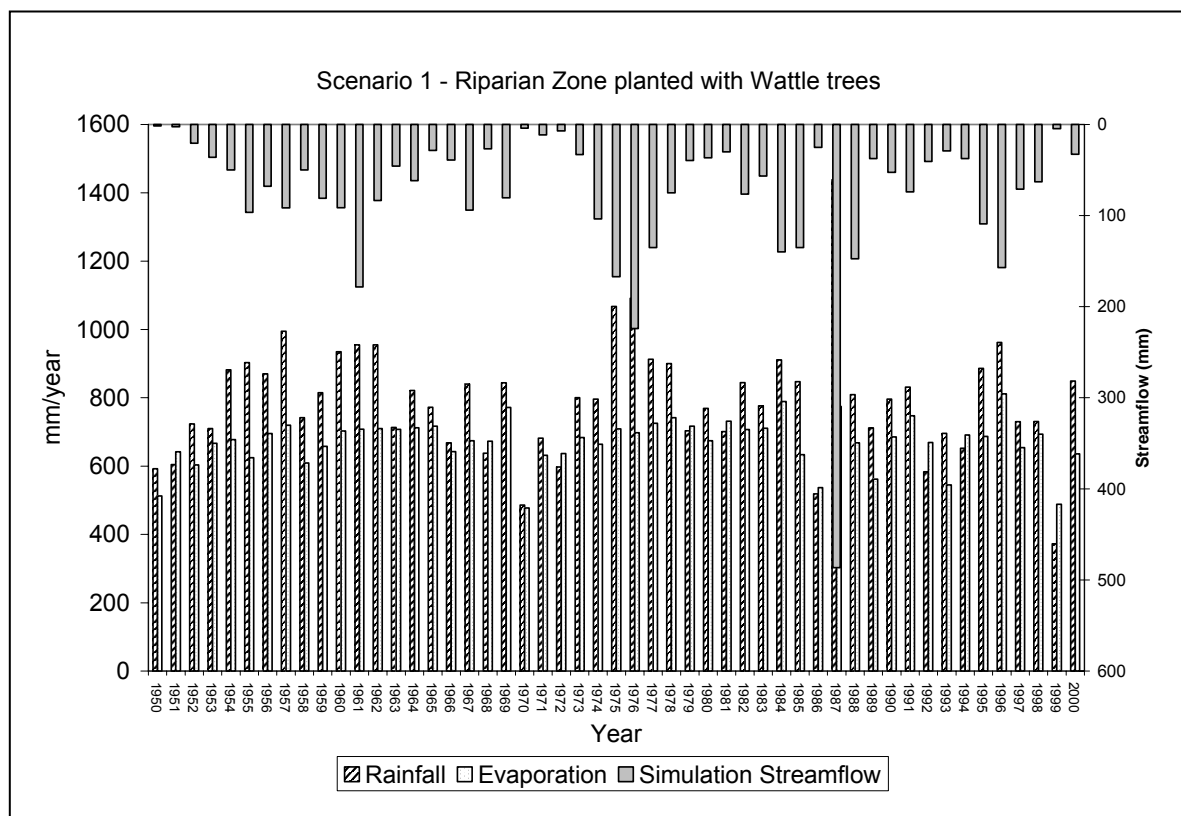


**Figure 4.31.** Streamflow, rainfall and evaporation for a fifty year period for the Two Streams Catchment A.

Recorded streamflow in 2000 was 20 mm compared with 32 mm predicted by the SWAT model. From these data we concluded that the model was predicting annual streamflow with reasonable accuracy. Annual evaporation for the Wattle trees varied between 600 mm in dry years to over 800 mm in wet years for the completely afforested catchment. Evaporation only exceeded rainfall in the very dry years of the simulation (e.g. 1999). Annual streamflow for the three different scenarios and the accumulated totals (Figures 4.31 and 4.32) showed that the streamflow was reduced by the wattle trees when compared with the natural veld scenario.

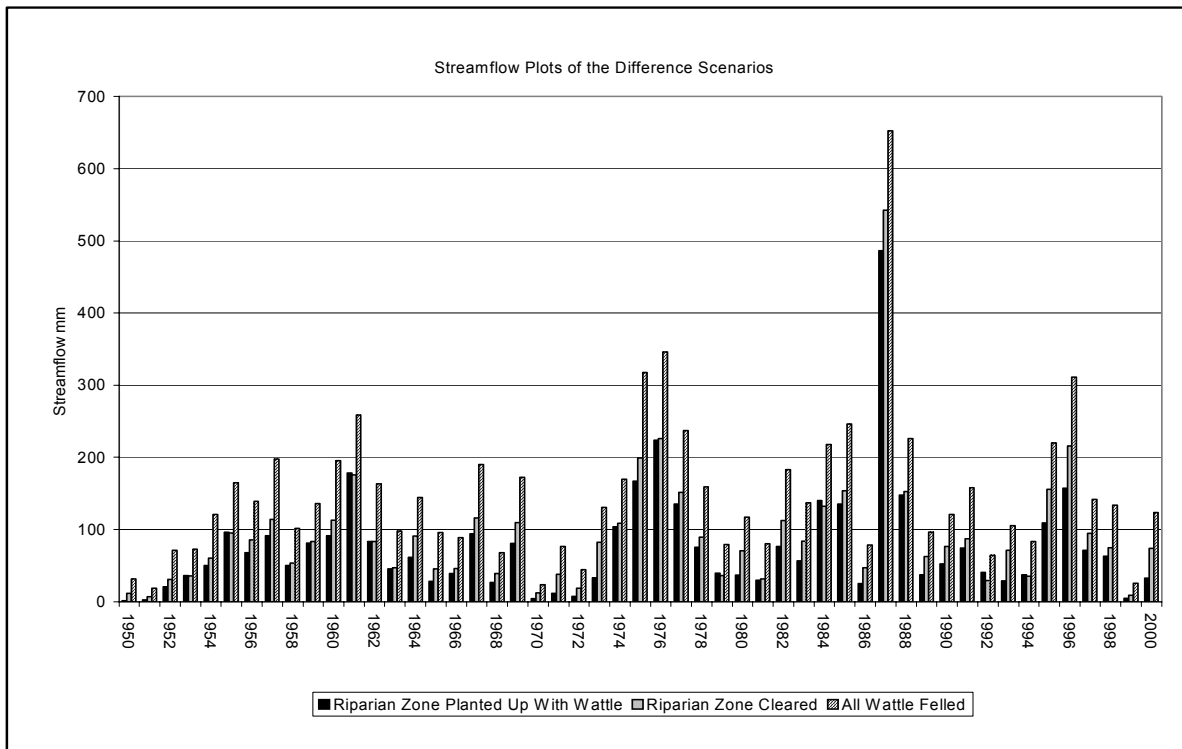


**Figure 4.32.** Annual predicted streamflow for the three different scenarios.

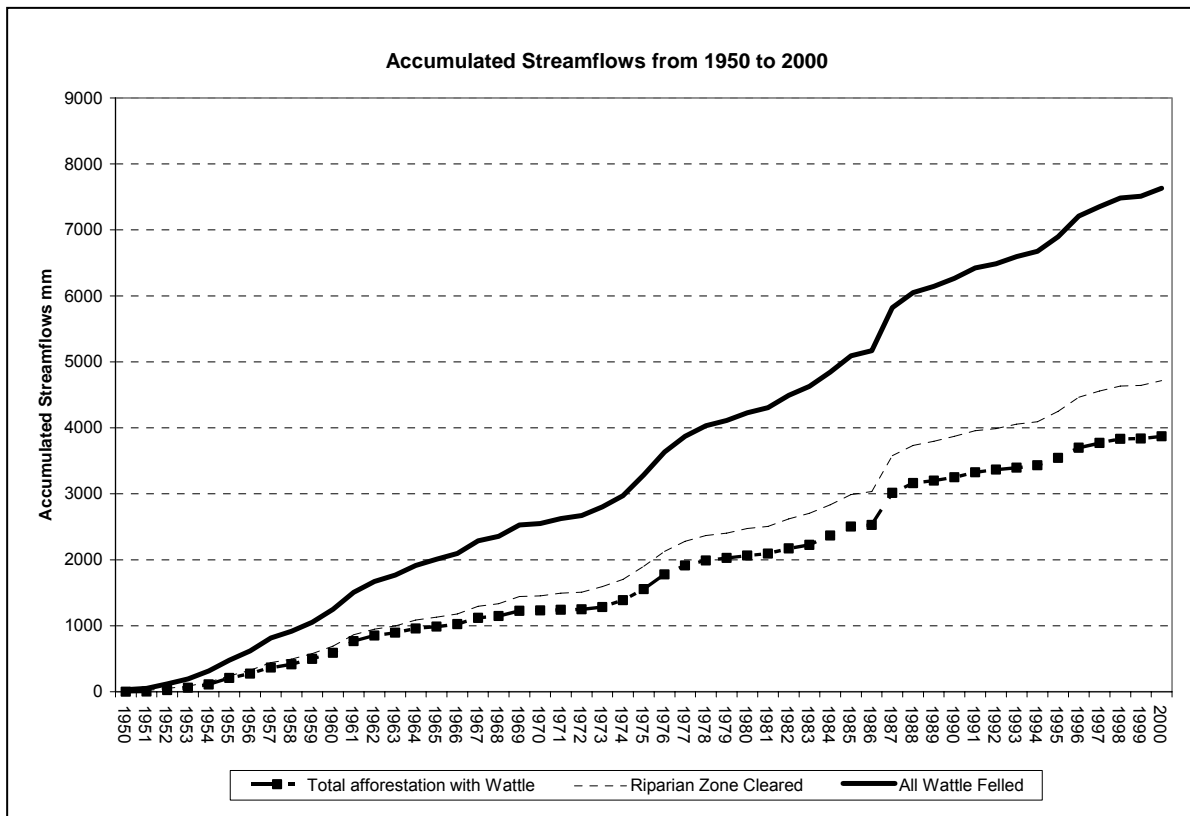


**Figure 4.33.** Accumulated streamflows for the three different scenarios

Removal of the riparian trees was also evidenced by an increase in streamflow when compared with the total afforestation (Figure 16). A double mass balance plot of these data (accumulated streamflow vs accumulated rainfall) showed the same trends (Figure 4.33). The total increase in predicted streamflow caused by the removal of the riparian trees over the fifty year period was 346 mm or about 17 mm annum<sup>-1</sup>.

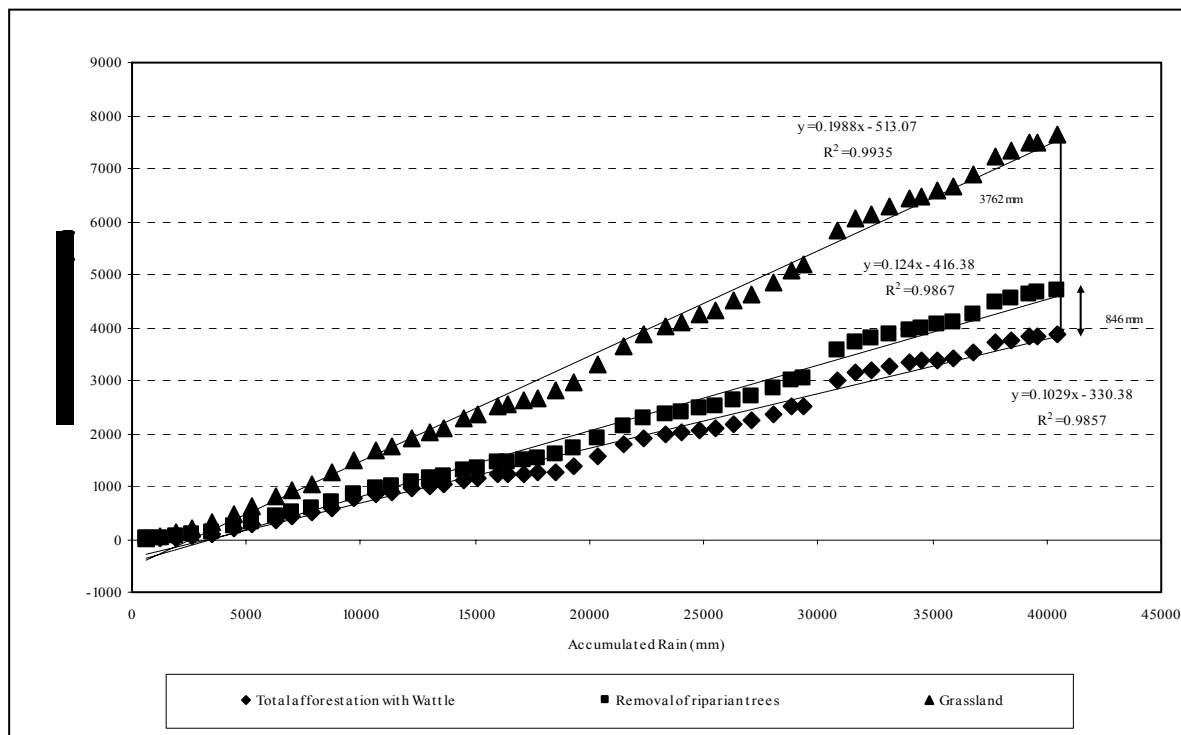


**Figure 4.33.** Rainfall runoff relationships for catchment A for three different scenarios (1950-2000).

The removal of the riparian trees over the fifty year period was 346 mm or about 17 mm annum<sup>-1</sup>. This compares with the 35 mm increase actually measured over the three year period following the post riparian clearing operation (i.e. 12 mm annum<sup>-1</sup>). Modelled and measured predictions were therefore in close agreement. The difference between the total afforestation and natural veld over the 50 year simulation was 3762 mm or about 75 mm annum<sup>-1</sup>.

#### 4.10 Conclusions

The data collected in this study have demonstrated the impact of both riparian and upland wattle on the streamflow of a small catchment in the KwaZulu Natal midlands. Initial results show that the streamflow reduction resulting from the combined effects of the riparian and upslope wattle trees is a decrease in runoff of approximately 60 %. Both the ACRU and SWAT models have been successfully validated using the Two Streams catchment A data sets. The models showed a streamflow reduction of about 75 mm annum<sup>-1</sup>, when compared with natural grassland. The modelled data were in close agreement with the measured data.

#### 5. Acknowledgements

The project team would like to gratefully acknowledge the funding agencies who made this work possible: namely the WRC and DWAF (WfW). The sustained efforts of the field staff, Joshua Xaba, Alistair Clulow, Zaheer Rasool, Lucas Ngidi and Vivek Naiken) to gather the data are also acknowledged.